Journal of the Mechanics and Physics of Solids 60 (2012) 261–276

Contents lists available at SciVerse ScienceDirect

Journal of the Mechanics and Physics of Solids

journal homepage: www.elsevier.com/locate/jmps

Strain gradient solution for the Eshelby-type polyhedral inclusion problem

X.-L. Gao [a,*], M.Q. Liu [b]

[a] Department of Mechanical Engineering, University of Texas at Dallas, 800 West Campbell Road, Richardson, TX 75080-3021, USA
[b] Department of Mechanical Engineering, Texas A&M University, College Station, TX 77843-3123, USA

ARTICLE INFO

Article history:
Received 22 July 2011
Received in revised form
27 October 2011
Accepted 28 October 2011
Available online 6 November 2011

Keywords:
Eshelby tensor
Polyhedral inclusion
Size effect
Eigenstrain
Strain gradient

ABSTRACT

The Eshelby-type problem of an arbitrary-shape polyhedral inclusion embedded in an infinite homogeneous isotropic elastic material is analytically solved using a simplified strain gradient elasticity theory (SSGET) that contains a material length scale parameter. The Eshelby tensor for a polyhedral inclusion of arbitrary shape is obtained in a general analytical form in terms of three potential functions, two of which are the same as the ones involved in the counterpart Eshelby tensor based on classical elasticity. These potential functions, as volume integrals over the polyhedral inclusion, are evaluated by dividing the polyhedral inclusion domain into tetrahedral duplexes, with each duplex and the associated local coordinate system constructed using a procedure similar to that employed by Rodin (1996. J. Mech. Phys. Solids 44, 1977–1995). Each of the three volume integrals is first transformed to a surface integral by applying the divergence theorem, which is then transformed to a contour (line) integral based on Stokes' theorem and using an inverse approach different from those adopted in the existing studies based on classical elasticity. The newly derived SSGET-based Eshelby tensor is separated into a classical part and a gradient part. The former contains Poisson's ratio only, while the latter includes the material length scale parameter additionally, thereby enabling the interpretation of the inclusion size effect. This SSGET-based Eshelby tensor reduces to that based on classical elasticity when the strain gradient effect is not considered. For homogenization applications, the volume average of the new Eshelby tensor over the polyhedral inclusion is also provided in a general form. To illustrate the newly obtained Eshelby tensor and its volume average, three types of polyhedral inclusions – cubic, octahedral and tetrakaidecahedral – are quantitatively studied by directly using the general formulas derived. The numerical results show that the components of the SSGET-based Eshelby tensor for each of the three inclusion shapes vary with both the position and the inclusion size, while their counterparts based on classical elasticity only change with the position. It is found that when the inclusion is small, the contribution of the gradient part is significantly large and should not be neglected. It is also observed that the components of the averaged Eshelby tensor based on the SSGET change with the inclusion size: the smaller the inclusion, the smaller the components. When the inclusion size becomes sufficiently large, these components are seen to approach (from below) the values of their classical elasticity-based counterparts, which are constants independent of the inclusion size.

* Corresponding author. Tel.: +1 972 883 4550; fax: +1 972 883 4659.
E-mail address: Xin-Lin.Gao@utdallas.edu (X.-L. Gao).

0022-5096/$ - see front matter © 2011 Elsevier Ltd. All rights reserved.
doi:10.1016/j.jmps.2011.10.010

Report Documentation Page

Form Approved
OMB No. 0704-0188

1. REPORT DATE	2. REPORT TYPE	3. DATES COVERED
2012		**00-00-2012 to 00-00-2012**

4. TITLE AND SUBTITLE	5a. CONTRACT NUMBER
Strain gradient solution for the Eshelby-type polyhedral inclusion problem	5b. GRANT NUMBER
	5c. PROGRAM ELEMENT NUMBER
6. AUTHOR(S)	5d. PROJECT NUMBER
	5e. TASK NUMBER
	5f. WORK UNIT NUMBER
7. PERFORMING ORGANIZATION NAME(S) AND ADDRESS(ES) **Texas A&M University,Department of Mechanical Engineering,College Station,TX,77843**	8. PERFORMING ORGANIZATION REPORT NUMBER
9. SPONSORING/MONITORING AGENCY NAME(S) AND ADDRESS(ES)	10. SPONSOR/MONITOR'S ACRONYM(S)
	11. SPONSOR/MONITOR'S REPORT NUMBER(S)

12. DISTRIBUTION/AVAILABILITY STATEMENT
Approved for public release; distribution unlimited

13. SUPPLEMENTARY NOTES

14. ABSTRACT

The Eshelby-typeproblemofanarbitrary-shapepolyhedralinclusionembeddedinan infinitehomogeneousisotropicelasticmaterialisanalyticallysolvedusingasimplified strain gradientelasticitytheory(SSGET)thatcontainsamateriallengthscalepara-meter.TheEshelbytensorforapolyhedralinclusionofarbitraryshapeisobtainedina generalanalyticalformintermsofthreepotentialfunctions,twoofwhicharethesame as theonesinvolvedinthecounterpartEshelbytensorbasedonclassicalelasticity. Thesepotentialfunctions,asvolumeintegralsoverthepolyhedralinclusion,are evaluatedbydividingthepolyhedralinclusiondomainintotetrahedralduplexes,with each duplexandtheassociatedlocalcoordinatesystemconstructedusingaprocedure similartothatemployedbyRodin(1996.J.Mech.Phys.Solids44,1977?1995).Eachof the threevolumeintegralsisfirsttransformedtoasurfaceintegralbyapplyingthe divergencetheorem,whichisthentransformedtoacontour(line)integralbasedon Stokes? theoremandusinganinverseapproachdifferentfromthoseadoptedinthe existingstudiesbasedonclassicalelasticity.ThenewlyderivedSSGET-basedEshelby tensor isseparatedintoaclassicalpartandagradientpart.Theformercontains Poisson?sratioonly,whilethelatterincludesthemateriallengthscaleparameter additionally,therebyenablingtheinterpretationoftheinclusionsizeeffect.ThisSSGET-basedEshelbytensorreducestothatbasedonclassicalelasticitywhenthestrain gradienteffectisnotconsidered.Forhomogenizationapplications,thevolumeaverage of thenewEshelbytensoroverthepolyhedralinclusionisalsoprovidedinageneral form. ToillustratethenewlyobtainedEshelbytensoranditsvolumeaverage,three types ofpolyhedralinclusions?cubic,octahedralandtetrakaidecahedral?are quantitativelystudiedbydirectlyusingthegeneralformulasderived.Thenumerical results showthatthecomponentsoftheSSGET-basedEshelbytensorforeachofthe threeinclusionshapesvarywithboththepositionandtheinclusionsize,whiletheir counterpartsbasedonclassicalelasticityonlychangewiththeposition.Itisfoundthat when theinclusionissmall,thecontributionofthegradientpartissignificantlylarge and shouldnotbeneglected.Itisalsoobservedthatthecomponentsoftheaveraged EshelbytensorbasedontheSSGETchangewiththeinclusionsize:thesmallerthe inclusion,thesmallerthecomponents.Whentheinclusionsizebecomessufficiently large, thesecomponentsareseentoapproach(frombelow)thevaluesoftheirclassical elasticity-basedcounterparts,whichareconstantsindependentoftheinclusionsize.

15. SUBJECT TERMS

16. SECURITY CLASSIFICATION OF:			17. LIMITATION OF ABSTRACT	18. NUMBER OF PAGES	19a. NAME OF RESPONSIBLE PERSON
a. REPORT	b. ABSTRACT	c. THIS PAGE			
unclassified	**unclassified**	**unclassified**	**Same as Report (SAR)**	**16**	

1. Introduction

Eshelby's (1957, 1959) solution for the problem of an infinite homogeneous isotropic elastic material containing an ellipsoidal inclusion prescribed with a uniform eigenstrain is a milestone in micromechanics. The solution for the dynamic Eshelby ellipsoidal inclusion problem was obtained by Michelitsch et al. (2003), which reduces to the Eshelby solution in the static limiting case. Both of these solutions are based on classical elasticity. Recently, the Eshelby ellipsoidal inclusion problem was solved by Gao and Ma (2010b) using a simplified strain gradient elasticity theory, which recovers Eshelby's (1957, 1959) solution when the strain gradient effect is not considered.

A remarkable property of Eshelby's (1957) solution is that the Eshelby tensor, which is a fourth-order strain transformation tensor directly linking the induced strain to the prescribed uniform eigenstrain, is constant inside the inclusion. However, this property is true only for ellipsoidal inclusions (and when classical elasticity is used), which is known as the Eshelby conjecture (e.g., Eshelby, 1961; Rodin, 1996; Markenscoff, 1998a,b; Lubarda and Markenscoff, 1998; Liu, 2008; Li and Wang, 2008; Gao and Ma, 2010b; Ammari et al., 2010).

For non-ellipsoidal polyhedral inclusions, Rodin (1996) provided an algorithmic analytical solution and showed that Eshelby's tensor cannot be constant inside a polyhedral inclusion, thereby proving the Eshelby conjecture in the case of polyhedral inclusions. The expressions of Eshelby's tensor for two-dimensional (2-D) polygonal inclusions were included in Rodin (1996). The explicit expressions of the Eshelby tensor for three-dimensional (3-D) polyhedral inclusions were later derived by Nozaki and Taya (2001), where an exact solution for the stress field inside and outside an arbitrary-shape polyhedral inclusion was obtained and numerical results for five regular polyhedral inclusion shapes and three other shapes of the icosidodeca family were presented. Both Rodin (1996) and Nozaki and Taya (2001) made use of an algorithm developed by Waldvogel (1979) for evaluating the Newtonian (harmonic) potential over a polyhedral body. A more compact form of the Eshelby tensor than that presented in Nozaki and Taya (2001) for a polyhedral inclusion in an infinite elastic space was proposed by Kuvshinov (2008) using a coordinate-invariant formulation, where problems of polyhedral inclusions in an elastic half-space and bi-materials were also investigated. In addition, specific analytical solutions have been obtained for polyhedral inclusions of simple shapes such as cuboids (e.g., Chiu, 1977; Lee and Johnson, 1978; Liu and Wang, 2005) and pyramids (e.g., Pearson and Faux, 2000; Glas, 2001; Nenashev and Dvurechenskil, 2010). Also, illustrative results have been provided for dynamic Eshelby problems of cubic and triangularly prismatic inclusions along with spherical and ellipsoidal ones by Wang et al. (2005) using their general solution for the dynamic Eshelby problem for inclusions of various shapes.

However, these existing studies on polyhedral inclusion problems are all based on the classical elasticity theory, which does not contain any material length scale parameter. As a result, the Eshelby tensors obtained in these studies and the subsequent homogenization methods cannot capture the inclusion (particle) size effect on elastic properties exhibited by particle–matrix composites (e.g., Vollenberg and Heikens, 1989; Cho et al., 2006; Marcadon et al., 2007). Solutions for polyhedral inclusion problems are also important for describing interpenetrating phase composites reinforced by 3-D networks (e.g., Poniznik et al., 2008; Jhaver and Tippur, 2009) and for understanding semiconductor materials buried with quantum dots that are typically polyhedral-shaped (e.g., Kuvshinov, 2008; Nenashev and Dvurechenskil, 2010). These materials often exhibit microstructure-dependent size effects whose interpretation requires the use of higher-order continuum theories.

In this paper, the Eshelby-type inclusion problem of a polyhedral inclusion prescribed with a uniform eigenstrain and a uniform eigenstrain gradient and embedded in an infinite homogeneous isotropic elastic material is solved using a simplified strain gradient elasticity theory (SSGET) (e.g., Gao and Park, 2007), which contains a material length scale parameter and can describe size-dependent elastic deformations. The Eshelby tensor is analytically obtained in terms of three potential functions, two of which are the same as the ones involved in the counterpart Eshelby tensor based on classical elasticity. These potential functions, as three volume integrals over the polyhedral inclusion, are evaluated by dividing the polyhedral inclusion domain into tetrahedral duplexes. Each duplex and the associated local coordinate system are constructed using a procedure similar to that developed by Rodin (1996) based on the algorithm proposed in Waldvogel (1979). Each of the three volume integrals is first transformed to a surface integral by applying the divergence theorem, which is then transformed to a contour (line) integral based on Stokes' theorem and using an inverse approach different from those employed in the existing studies for evaluating the two integrals involved in the classical elasticity-based Eshelby tensor for a polyhedral inclusion.

The rest of this paper is organized as follows. In Section 2, the general form of the Eshelby tensor for a 3-D arbitrary-shape inclusion based on the SSGET is presented in terms of three potential functions (volume integrals). The expressions of the SSGET-based Eshelby tensor for a polyhedral inclusion of arbitrary shape are analytically derived in Section 3, which is separated into a classical part and a gradient part. The averaged Eshelby tensor over the inclusion volume is also analytically evaluated there. Numerical results are provided in Section 4 to quantitatively illustrate the position and inclusion size dependence of the newly obtained Eshelby tensor for the polyhedral inclusion problem. The paper concludes in Section 5.

2. Eshelby tensor based on the SSGET

The SSGET is the simplest strain gradient elasticity theory evolving from Mindlin's pioneering work. It is also known as the first gradient elasticity theory of Helmholtz type and the dipolar gradient elasticity theory (e.g., Gao and Ma, 2010a).

According to the SSGET (Gao and Park, 2007; Gao and Ma, 2010a), the Navier-like displacement equations of equilibrium are given by

$$(\lambda+\mu)u_{i,ij}+\mu u_{j,kk}-L^2[(\lambda+\mu)u_{i,ij}+\mu u_{j,kk}]_{,mm}+f_j=0 \text{ in } \Omega, \tag{1}$$

and the boundary conditions have the form:

$$\left.\begin{array}{l}\sigma_{ij}n_j-(\mu_{ijk}n_k)_{,j}+(\mu_{ijk}n_kn_l)_{,l}n_j=\overline{t}_i \text{ or } u_i=\overline{u}_i\\ \mu_{ijk}n_jn_k=\overline{q}_i \text{ or } u_{i,l}n_l=\frac{\overline{\partial u_i}}{\partial n}\end{array}\right\} \text{ on } \partial\Omega, \tag{2}$$

where λ and μ are the Lamé constants in classical elasticity, L is a material length scale parameter, u_i are the components of the displacement vector, f_i are the components of the body force vector (force per unit volume), σ_{ij} are the components of the total stress, $\boldsymbol{\sigma}=\sigma_{ij}\mathbf{e}_i\otimes\mathbf{e}_j$, μ_{ijk} are the components of the double stress, $\boldsymbol{\mu}=\mu_{ijk}\mathbf{e}_i\otimes\mathbf{e}_j\otimes\mathbf{e}_k$, and t_i and q_i are, respectively, the components of the Cauchy traction vector and double stress traction vector. Also, in Eqs. (1) and (2), Ω is the region occupied by the elastically deformed material, $\partial\Omega$, is the smooth bounding surface of Ω, n_i is the outward unit normal vector on $\partial\Omega$, and the overhead bar represents the prescribed value. In addition,

$$\mu_{ijk}=L^2\tau_{ij,k}=\mu_{jik}, \quad \sigma_{ij}\equiv\tau_{ij}-\mu_{ijk,k}=\tau_{ij}-L^2\tau_{ij,kk}=\sigma_{ji}, \tag{3}$$

where τ_{ij} are the components of the Cauchy stress, $\boldsymbol{\tau}=\tau_{ij}\mathbf{e}_i\otimes\mathbf{e}_j$.

When the strain gradient effect is not considered (i.e., $L=0$), $\mu_{ijk}=0$ and $\sigma_{ij}=\tau_{ij}$ (see Eq. (3)), and Eqs. (1) and (2) reduce to the governing equations and the boundary conditions in terms of displacement in classical elasticity (e.g., Timoshenko and Goodier, 1970; Gao and Rowlands, 2000).

Note that the standard index notation, together with the Einstein summation convention, is used in Eqs. (1), (2) and (3) and throughout this paper, with each Latin index (subscript) ranging from 1 to 3 unless otherwise stated.

Solving Eq. (1), subject to the boundary conditions of u_i and their first, second and third derivatives vanishing at infinity, gives the fundamental solution and Green's function based on the SSGET. By using 3-D Fourier and inverse Fourier transforms, the fundamental solution of Eq. (1) has been obtained as (Gao and Ma, 2009)

$$u_i(\mathbf{x})=\iiint_{-\infty}^{+\infty}G_{ij}(\mathbf{x}-\mathbf{y})f_j(\mathbf{y})d\mathbf{y}, \tag{4}$$

where $\mathbf{x}$ is the position vector of a point in the infinite 3-D space, $\mathbf{y}$ is the integration point, and $G_{ij}(\cdot)$ is Green's function (a second-order tensor) given by

$$G_{ij}(\mathbf{x})=\frac{1}{16\pi\mu(1-\nu)}[A(x)\delta_{ij}-B(x)_{,ij}], \tag{5}$$

with

$$A(x)\equiv 4(1-\nu)\frac{1}{x}\left(1-e^{-x/L}\right), \quad B(x)\equiv x+\frac{2L^2}{x}-\frac{2L^2}{x}e^{-x/L}. \tag{6}$$

When $L=0$, Eqs. (5) and (6) reduce to the Green's function for 3-D problems in classical elasticity (e.g., Li and Wang, 2008). In Eqs. (5) and (6), ν is Poisson's ratio, which is related to the Lamé constants λ and μ through (e.g., Timoshenko and Goodier, 1970)

$$\lambda=\frac{E\nu}{(1+\nu)(1-2\nu)}, \quad \mu=\frac{E}{2(1+\nu)}, \tag{7}$$

where E is Young's modulus.

By using the Green's function method entailing Eqs. (4), (5) and (6), the general expressions of the Eshelby tensor based on the SSGET can then be obtained, as summarized below.

Consider the problem of a 3-D inclusion of arbitrary shape embedded in an infinite homogenous isotropic elastic body. The inclusion is prescribed with a uniform eigenstrain $\boldsymbol{\varepsilon}^*$ and a uniform eigenstrain gradient $\boldsymbol{\kappa}^*$. There is no body force or any other external force acting on the elastic body. The disturbed strain, ε_{ij}, induced by $\boldsymbol{\varepsilon}^*$ and $\boldsymbol{\kappa}^*$ can be shown to be (Gao and Ma, 2009, 2010b)

$$\varepsilon_{ij}=S_{ijkl}\varepsilon^*_{kl}+T_{ijklm}\kappa^*_{klm}, \tag{8}$$

where S_{ijkl} is the fourth-order Eshelby tensor having 36 independent components, and T_{ijklm} is a fifth-order Eshelby-like tensor with 108 independent components. Eq. (8) shows that $\boldsymbol{\varepsilon}$ $(=\varepsilon_{ij}\mathbf{e}_i\otimes\mathbf{e}_j)$ is solely linked to $\boldsymbol{\varepsilon}^*$ in the absence of $\boldsymbol{\kappa}^*$ (i.e., the classical case) and is fully related to $\boldsymbol{\kappa}^*$ when $\boldsymbol{\varepsilon}^*=\mathbf{0}$. The fourth-order Eshelby tensor has been obtained as

$$S_{ijkl}=S^C_{ijkl}+S^G_{ijkl}, \tag{9a}$$

$$S^C_{ijkl}=\frac{1}{8\pi(1-\nu)}[\Phi_{,ijkl}-2\nu\Lambda_{,ij}\delta_{kl}-(1-\nu)(\Lambda_{,lj}\delta_{ik}+\Lambda_{,kj}\delta_{il}+\Lambda_{,li}\delta_{jk}+\Lambda_{,ki}\delta_{jl})], \tag{9b}$$

$$S^G_{ijkl}=\frac{1}{8\pi(1-\nu)}[2\nu\Gamma_{,ij}\delta_{kl}+(1-\nu)(\Gamma_{,jl}\delta_{ik}+\Gamma_{,il}\delta_{jk}+\Gamma_{,jk}\delta_{il}+\Gamma_{,ik}\delta_{jl})+2L^2(\Lambda_{,ijkl}-\Gamma_{,ijkl})], \tag{9c}$$

where S^C_{ijkl} is the classical part, S^G_{ijkl} is the gradient part, δ_{ij} is the Kronecker delta, and

$$\Phi(\mathbf{x}) = \int_\Omega |\mathbf{x}-\mathbf{y}|\, d\mathbf{y}, \tag{10a}$$

$$\Lambda(\mathbf{x}) = \int_\Omega \frac{1}{|\mathbf{x}-\mathbf{y}|}\, d\mathbf{y}, \tag{10b}$$

$$\Gamma(\mathbf{x}) = \int_\Omega \frac{e^{-|\mathbf{x}-\mathbf{y}|/L}}{|\mathbf{x}-\mathbf{y}|}\, d\mathbf{y} \tag{10c}$$

are three scalar-valued potential functions that can be obtained analytically or numerically by evaluating the volume integrals over the domain Ω occupied by the inclusion, with $|\mathbf{x}| = x = (x_k x_k)^{1/2}$ and $\mathbf{y}$ ($\in \Omega$) being the integration variable. Note that the first two potential functions given in Eqs. (10a) and (10b) are the same as the ones involved in the Eshelby tensor based on classical elasticity (e.g., Mura, 1987; Nemat-Nasser and Hori, 1999; Li and Wang, 2008), whereas the third one defined in Eq. (10c) results from the use of the SSGET. It should be mentioned that $\Phi(\mathbf{x})$ in Eq. (10a) and $\Lambda(\mathbf{x})$ in Eq. (10b) are, respectively, known to be a biharmonic potential and a Newtonian potential (e.g., Li and Wang, 2008), while a variant of $\Gamma(\mathbf{x})$ in Eq. (10c) is called the Yukawa potential in physics (e.g., Rowlinson, 1989).

Eqs. (10a), (10b) and (10c) show that among the three potential functions, only the third one, $\Gamma(\mathbf{x})$, involves the length scale parameter L. It then follows from Eqs. (9c), (10b) and (10c) that S^G_{ijkl} depends on L, while S^C_{ijkl}, expressed in terms of $\Lambda(\mathbf{x})$ and $\Phi(\mathbf{x})$ only according to Eqs. (9b), (10a) and (10b), is independent of L. Also, it is seen from Eqs. (9c), (10b) and (10c) that $S^G_{ijkl}=0$ when $L=0$ (and thus $\Gamma(\mathbf{x})\equiv 0$), thereby giving $S_{ijkl} = S^C_{ijkl}$ (from Eq. (9a)). That is, the Eshelby tensor derived using the SSGET reduces to that based on classical elasticity when the strain gradient effect is not considered.

The fifth-order Eshelby-like tensor $\mathbf{T}$, which relates the eigenstrain gradient $\boldsymbol{\kappa}^*$ to the disturbed strain $\boldsymbol{\varepsilon}$ in the elastic body (see Eq. (8)), can be shown to be

$$T_{ijklm} = \frac{L^2}{8\pi(1-\nu)}[2\nu\Psi_{,ijm}\delta_{kl} + (1-\nu)(\Psi_{,lmi}\delta_{jk} + \Psi_{,lmj}\delta_{ik} + \Psi_{,kmi}\delta_{jl} + \Psi_{,kmj}\delta_{il}) - \Pi_{,ijklm}], \tag{11}$$

where

$$\Psi(\mathbf{x}) \equiv \Lambda - \Gamma, \quad \Pi(\mathbf{x}) \equiv \Phi + 2L^2(\Lambda - \Gamma), \tag{12a,b}$$

with the scalar-valued potential functions $\Phi(\mathbf{x})$, $\Lambda(\mathbf{x})$ and $\Gamma(\mathbf{x})$ defined in Eqs. (10a), (10b) and (10c). It is clear from Eq. (11) that $\mathbf{T}$ vanishes when $L=0$. Then, with $S_{ijkl} = S^C_{ijkl}$ as discussed above, Eq. (8) simply becomes $\varepsilon_{ij} = S^C_{ijkl}\varepsilon^*_{kl}$ when $L=0$, which is the defining relation for the Eshelby tensor based on classical elasticity (Eshelby, 1957), as expected.

Eqs. (9a), (9b), (9c) and (11) provide the general formulas for determining S_{ijkl} ($= S^C_{ijkl} + S^G_{ijkl}$) and T_{ijklm} for an inclusion of arbitrary shape in terms of the potential functions $\Lambda(\mathbf{x})$, $\Phi(\mathbf{x})$ and $\Gamma(\mathbf{x})$ defined in Eqs. (10a), (10b) and (10c). For the cases of a spherical inclusion, a cylindrical inclusion and an ellipsoidal inclusion in an infinite elastic medium, analytical expressions have been obtained for $\Lambda(\mathbf{x})$, $\Phi(\mathbf{x})$ and $\Gamma(\mathbf{x})$ and thus for the Eshelby tensor (Gao and Ma, 2009, 2010b; Ma and Gao, 2010). The more complex case of a polyhedral inclusion of arbitrary shape, for which $\Lambda(\mathbf{x})$, $\Phi(\mathbf{x})$ and $\Gamma(\mathbf{x})$ are difficult to evaluate analytically, is examined in this study.

3. Polyhedral inclusion

The problem of an arbitrary-shape polyhedral inclusion in an infinite elastic body has been analytically studied by Rodin (1996), Nozaki and Taya (2001) and Kuvshinov (2008) using classical elasticity. The Eshelby tensor for this problem is derived here using the SSGET-based general formulas and a new method for evaluating the potential functions $\Lambda(\mathbf{x})$, $\Phi(\mathbf{x})$ and $\Gamma(\mathbf{x})$.

3.1. Eshelby tensor

Consider an arbitrarily shaped polyhedral inclusion embedded in an infinite homogeneous isotropic elastic material. The polyhedral inclusion has p faces and is prescribed with a uniform eigenstrain $\boldsymbol{\varepsilon}^*$ and a uniform eigenstrain gradient $\boldsymbol{\kappa}^*$.

The p-faced polyhedral domain occupied by the inclusion can be divided into tetrahedral duplexes originated from a chosen (arbitrary) point $\mathbf{x}$ (Waldvogel, 1979; Rodin, 1996). Each duplex can be further divided into two simplexes, each of which is a tetrahedron with three of its four faces being right triangles (see Fig. 1). The four vertices of each of the duplexes are, respectively, the projection point of $\mathbf{x}$ on a polyhedral surface (i.e., $\mathbf{x}_I$), two adjacent vertices on this surface (i.e., $\mathbf{V}^+_{JI}$ and $\mathbf{V}^-_{JI}$), and the point $\mathbf{x}$ itself. For each of these duplexes, a local Cartesian coordinate system is constructed, with point $\mathbf{x}$ being set as the origin. The three orthogonal axes of the local coordinate system are denoted by λ, η and ζ, respectively. The coordinates of the two vertices $\mathbf{V}^+_{JI}$ and $\mathbf{V}^-_{JI}$ on the Jth edge of the Ith surface are, respectively, given by (b_{JI}, l^+_{JI}, a_I) and (b_{JI}, l^-_{JI}, a_I), as shown in Fig. 2.

In Fig. 2, $\boldsymbol{\lambda}^0_{JI}$, $\boldsymbol{\eta}^0_{JI}$ and $\boldsymbol{\zeta}^0_I$ are the unit vectors associated with the local coordinates λ_{JI}, η_{JI} and ζ_I, $\mathbf{y}$ is an arbitrary point on the Jth edge of the Ith surface, $\mathbf{r}$ is the position vector of $\mathbf{y}$ relative to the origin $\mathbf{x}$ (i.e., $\mathbf{r}=\mathbf{y}-\mathbf{x}$), and $\mathbf{r}^s_I$ is the projection of $\mathbf{r}$ on the Ith surface. The usual Cartesian coordinates (x_1, x_2, x_3) are used in the global coordinate system having $(\mathbf{e}_1, \mathbf{e}_2, \mathbf{e}_3)$ as the associated base vectors.

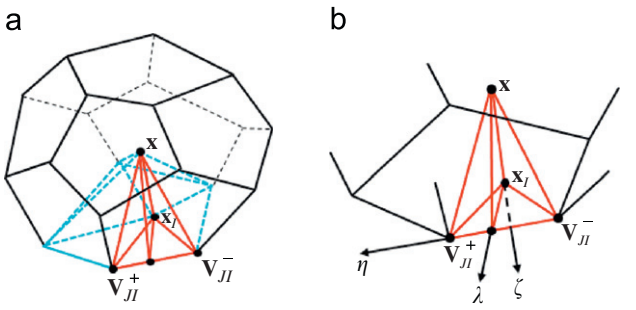

Fig. 1. A polyhedron represented by duplexes: (a) a polyhedron (with five duplexes shown); (b) a duplex and the associated local coordinate system constructed from an arbitrary point **x**.

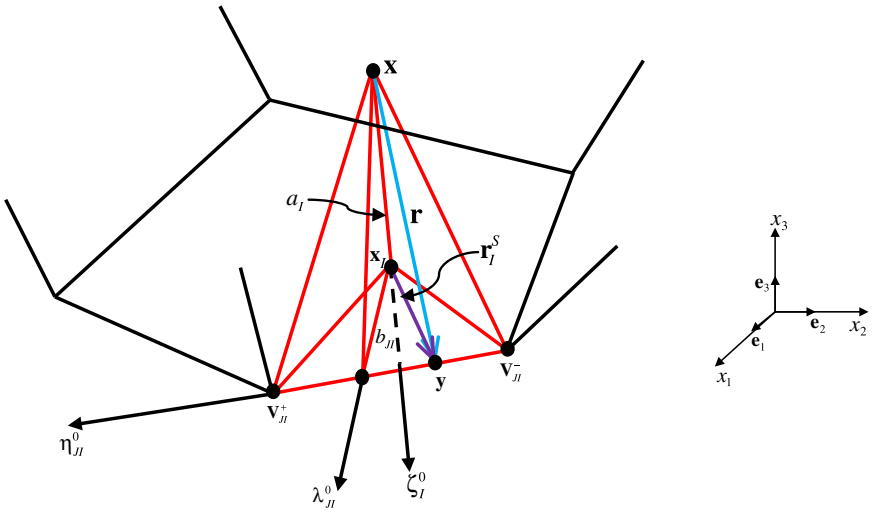

Fig. 2. A duplex with its base on the *I*th surface and one local coordinate axis (η) along the *J*th edge of the *I*th surface.

To obtain the Eshelby tensor for the polyhedral inclusion using Eqs. (9a), (9b) and (9c), the three potential functions $\Phi(\mathbf{x})$, $\Lambda(\mathbf{x})$ and $\Gamma(\mathbf{x})$ defined in Eqs. (10a), (10b) and (10c) are first evaluated over the polyhedral domain Ω using an approach different from those employed in Rodin (1996), Nozaki and Taya (2001) and Kuvshinov (2008) for evaluating $\Phi(\mathbf{x})$ and $\Lambda(\mathbf{x})$ involved in the classical elasticity-based Eshelby tensor, as shown next.

For a sufficiently smooth function $M(\mathbf{x}-\mathbf{y})$, the use of the divergence theorem gives

$$\frac{\partial}{\partial x_k}\iiint_\Omega M dV(\mathbf{y}) = -\iiint_\Omega \frac{\partial M}{\partial y_k} dV(\mathbf{y}) = -\sum_{I=1}^{p} (\zeta_I^0)_k \iint_{\partial\Omega_I} M dS(\mathbf{y}), \tag{13}$$

where p is the number of surfaces of the polyhedron, and $(\zeta_I^0)_k$ is the kth component of the unit outward normal vector on the Ith surface $\partial\Omega_I$, ζ_I^0.

To transform the surface integral in Eq. (13) to a contour (line) integral, let

$$M = (\nabla \times \mathbf{m})\cdot\zeta_I^0, \tag{14}$$

where $\mathbf{m}$ is a yet-unknown vector located on the Ith surface of the polyhedron, and $\nabla\times\mathbf{m}$ denotes the curl of $\mathbf{m}$. Using the Stokes theorem then yields, upon applying Eq. (14),

$$\iint_{\partial\Omega_I} M dS(\mathbf{y}) = \sum_{J=1}^{q} \int_{C_{JI}} \mathbf{m}\cdot\boldsymbol{\eta}_{JI}^0 dl, \tag{15}$$

where $\boldsymbol{\eta}_{JI}^0$ is the unit vector along the Jth boundary edge C_{JI} of the Ith surface.

Now, write

$$\mathbf{m} = \zeta_I^0 \times \left[\frac{\mathbf{r}_I^S}{r_I^S} g(r)\right], \tag{16}$$

where $r_I^S(=\sqrt{r^2-a_I^2}=|\mathbf{r}_I^S|)$ is the length of the projection of $\mathbf{r}$ on the Ith surface, and $g(r)$ is a function of $r\,(=|\mathbf{r}|)$ yet to be determined. Substituting Eq. (16) into Eq. (15) leads to

$$\iint_{\partial\Omega_I} M dS(\mathbf{y}) = \sum_{J=1}^{q} b_{JI} \int_{C_{JI}} \frac{g(r)}{r_I^S} dl, \tag{17}$$

where $b_{JI}\equiv \mathbf{r}_I^S\cdot\boldsymbol{\lambda}_{JI}^0$ is the distance from point $\mathbf{x}_I$ (the projection of point $\mathbf{x}$ on the Ith surface) to the Jth edge C_{JI} (see Fig. 2). For each specific function M, a different expression of $g(r)$ and thus $\mathbf{m}$ can be determined, as shown next for the three cases representing the integrands of the potential functions $\Phi(\mathbf{x})$, $\Lambda(\mathbf{x})$ and $\Gamma(\mathbf{x})$ defined in Eqs. (10a), (10b) and (10c).

For $M=r=|\mathbf{y}-\mathbf{x}|$ (corresponding to $\Phi(\mathbf{x})$), Eqs. (14) and (16) gives

$$r = g(r)\left(\nabla\cdot\frac{\mathbf{r}_I^S}{r_I^S}\right)+[\nabla g(r)]\cdot\frac{\mathbf{r}_I^S}{r_I^S}, \tag{18}$$

where ∇ is the gradient operator, and use has been made of the identity: $\mathbf{a}\times\mathbf{b}\times\mathbf{c}=(\mathbf{a}\cdot\mathbf{c})\mathbf{b}-(\mathbf{a}\cdot\mathbf{b})\mathbf{c}$, with $\mathbf{a}$, $\mathbf{b}$, $\mathbf{c}$ being arbitrary vectors and "$\times$", "$\cdot$" representing the cross, dot products, respectively. After carrying out the differentiation and dot product operations, Eq. (18) can be further simplified to

$$r = \frac{g(r)}{r_I^S}+g'(r)\frac{r_I^S}{r}, \tag{19}$$

where $g'(=dg/dr)$ is the first derivative of g with respect to r. The solution of Eq. (19) reads

$$g_\Phi(r) = \frac{r^3-a_I^3}{3r_I^S}, \tag{20}$$

where $a_I\,(=\mathbf{r}\cdot\boldsymbol{\zeta}_I^0)$ is the distance from point $\mathbf{x}$ to the Ith surface (see Fig. 2), and $g_\Phi(r)$ denotes the function $g(r)$ for the case with $M=r$.

Similarly, it can be shown that

$$g_\Lambda(r) = \frac{r_I^S}{r+a_I} \tag{21}$$

when $M=1/r=1/|\mathbf{y}-\mathbf{x}|$ (corresponding to $\Lambda(\mathbf{x})$), and

$$g_\Gamma(r) = \frac{L(e^{-a_I/L}-e^{-r/L})}{r_I^S} \tag{22}$$

when $M=e^{-r/L}/r=e^{-|\mathbf{y}-\mathbf{x}|/L}/|\mathbf{y}-\mathbf{x}|$ (corresponding to $\Gamma(\mathbf{x})$).

Using Eqs. (13), (17), (20), (21) and (22) in Eqs. (10a), (10b) and (10c) then leads to, with the local coordinate axis η being along the Jth edge,

$$\Phi_{,i} = -\sum_{I=1}^{p}\sum_{J=1}^{q}(\zeta_I^0)_i b_{JI}\int_{l_{JI}^-}^{l_{JI}^+}\frac{(a_I^2+b_{JI}^2+\eta^2)^{3/2}-a_I^3}{3(b_{JI}^2+\eta^2)}d\eta, \tag{23}$$

$$\Lambda_{,i} = -\sum_{I=1}^{p}\sum_{J=1}^{q}(\zeta_I^0)_i b_{JI}\int_{l_{JI}^-}^{l_{JI}^+}\frac{1}{\sqrt{a_I^2+b_{JI}^2+\eta^2}+a_I}d\eta, \tag{24}$$

$$\Gamma_{,i} = -\sum_{I=1}^{p}\sum_{J=1}^{q}(\zeta_I^0)_i b_{JI}\int_{l_{JI}^-}^{l_{JI}^+}\frac{L(e^{-a_I/L}-e^{-\sqrt{a_I^2+b_{JI}^2+\eta^2}/L})}{b_{JI}^2+\eta^2}d\eta, \tag{25}$$

where l_{JI}^+ and l_{JI}^- are, respectively, the coordinates of the two vertices $\mathbf{V}_{JI}^+$ and $\mathbf{V}_{JI}^-$ on the Jth edge, with l_{JI}^+ being positive and l_{JI}^- negative (see Fig. 2).

The integrals in Eqs. (23) and (24) can be exactly evaluated by direct integration to obtain the following closed-form expressions:

$$\Phi_{,i} = -\sum_{I=1}^{p}\sum_{J=1}^{q}(\zeta_I^0)_i\left\{\frac{l_{JI}^+ b_{JI}}{6}\sqrt{a_I^2+b_{JI}^2+(l_{JI}^+)^2}+\frac{a_I^3}{3}\tan^{-1}\left[\frac{a_I l_{JI}^+}{b_{JI}\sqrt{a_I^2+b_{JI}^2+(l_{JI}^+)^2}}\right]\right.$$
$$\left.-\frac{a_I^3}{3}\tan^{-1}\left(\frac{l_{JI}^+}{b_{JI}}\right)+\frac{3a_I^2 b_{JI}+b_{JI}^3}{6}\ln\left[\frac{l_{JI}^++\sqrt{a_I^2+b_{JI}^2+(l_{JI}^+)^2}}{\sqrt{a_I^2+b_{JI}^2}}\right]\right.$$

$$-\frac{l_{JI}^- b_{JI}}{6}\sqrt{a_I^2+b_{JI}^2+(l_{JI}^-)^2}-\frac{a_I^3}{3}\tan^{-1}\left[\frac{a_I l_{JI}^-}{b_{JI}\sqrt{a_I^2+b_{JI}^2+(l_{JI}^-)^2}}\right]+\frac{a_I^3}{3}\tan^{-1}\left(\frac{l_{JI}^-}{b_{JI}}\right)-\frac{3a_I^2 b_{JI}+b_{JI}^3}{6}\ln\left[\frac{l_{JI}^-+\sqrt{a_I^2+b_{JI}^2+(l_{JI}^-)^2}}{\sqrt{a_I^2+b_{JI}^2}}\right]\Bigg\}$$

$$\equiv-\sum_{I=1}^{p}\sum_{J=1}^{q}(\zeta_I^0)_i\Phi_1^{JI}=-\sum_{I=1}^{p}\sum_{J=1}^{q}(\zeta_I^0)_i[(\Phi_1^{JI})^+-(\Phi_1^{JI})^-], \tag{26}$$

$$\Lambda_{,i}=-\sum_{I=1}^{p}\sum_{J=1}^{q}(\zeta_I^0)_i\Bigg\{a_I\tan^{-1}\left[\frac{a_I l_{JI}^+}{b_{JI}\sqrt{a_I^2+b_{JI}^2+(l_{JI}^+)^2}}\right]-a_I\tan^{-1}\left(\frac{l_{JI}^+}{b_{JI}}\right)$$

$$+b_{JI}\ln\left[\frac{l_{JI}^++\sqrt{a_I^2+b_{JI}^2+(l_{JI}^+)^2}}{\sqrt{a_I^2+b_{JI}^2}}\right]-a_I\tan^{-1}\left[\frac{a_I l_{JI}^-}{b_{JI}\sqrt{a_I^2+b_{JI}^2+(l_{JI}^-)^2}}\right]+a_I\tan^{-1}\left(\frac{l_{JI}^-}{b_{JI}}\right)-b_{JI}\ln\left[\frac{l_{JI}^-+\sqrt{a_I^2+b_{JI}^2+(l_{JI}^-)^2}}{\sqrt{a_I^2+b_{JI}^2}}\right]\Bigg\}$$

$$\equiv-\sum_{I=1}^{p}\sum_{J=1}^{q}(\zeta_I^0)_i\Lambda_1^{JI}=-\sum_{I=1}^{p}\sum_{J=1}^{q}(\zeta_I^0)_i[(\Lambda_1^{JI})^+-(\Lambda_1^{JI})^-], \tag{27}$$

where Φ_1^{JI}, $(\Phi_1^{JI})^+$, $(\Phi_1^{JI})^-$, Λ_1^{JI}, $(\Lambda_1^{JI})^+$ and $(\Lambda_1^{JI})^-$ are functions defined by

$$\Phi_1^{JI}=\Phi_1^{JI}(a_I,b_{JI},l_{JI}^+,l_{JI}^-)=(\Phi_1^{JI})^+(a_I,b_{JI},l_{JI}^+)-(\Phi_1^{JI})^-(a_I,b_{JI},l_{JI}^-),$$

$$(\Phi_1^{JI})^+=\frac{l_{JI}^+ b_{JI}}{6}\sqrt{a_I^2+b_{JI}^2+(l_{JI}^+)^2}+\frac{a_I^3}{3}\tan^{-1}\left[\frac{a_I l_{JI}^+}{b_{JI}\sqrt{a_I^2+b_{JI}^2+(l_{JI}^+)^2}}\right]-\frac{a_I^3}{3}\tan^{-1}\left(\frac{l_{JI}^+}{b_{JI}}\right)$$

$$+\frac{3a_I^2 b_{JI}+b_{JI}^3}{6}\ln\left[\frac{l_{JI}^++\sqrt{a_I^2+b_{JI}^2+(l_{JI}^+)^2}}{\sqrt{a_I^2+b_{JI}^2}}\right],$$

$$(\Phi_1^{JI})^-=\frac{l_{JI}^- b_{JI}}{6}\sqrt{a_I^2+b_{JI}^2+(l_{JI}^-)^2}+\frac{a_I^3}{3}\tan^{-1}\left[\frac{a_I l_{JI}^-}{b_{JI}\sqrt{a_I^2+b_{JI}^2+(l_{JI}^-)^2}}\right]-\frac{a_I^3}{3}\tan^{-1}\left(\frac{l_{JI}^-}{b_{JI}}\right)$$

$$+\frac{3a_I^2 b_{JI}+b_{JI}^3}{6}\ln\left[\frac{l_{JI}^-+\sqrt{a_I^2+b_{JI}^2+(l_{JI}^-)^2}}{\sqrt{a_I^2+b_{JI}^2}}\right],$$

$$\Lambda_1^{JI}=\Lambda_1^{JI}(a_I,b_{JI},l_{JI}^+,l_{JI}^-)=(\Lambda_1^{JI})^+(a_I,b_{JI},l_{JI}^+)-(\Lambda_1^{JI})^-(a_I,b_{JI},l_{JI}^-),$$

$$(\Lambda_1^{JI})^+=a_I\tan^{-1}\left[\frac{a_I l_{JI}^+}{b_{JI}\sqrt{a_I^2+b_{JI}^2+(l_{JI}^+)^2}}\right]-a_I\tan^{-1}\left(\frac{l_{JI}^+}{b_{JI}}\right)+b_{JI}\ln\left[\frac{l_{JI}^++\sqrt{a_I^2+b_{JI}^2+(l_{JI}^+)^2}}{\sqrt{a_I^2+b_{JI}^2}}\right],$$

$$(\Lambda_1^{JI})^-=a_I\tan^{-1}\left[\frac{a_I l_{JI}^-}{b_{JI}\sqrt{a_I^2+b_{JI}^2+(l_{JI}^-)^2}}\right]-a_I\tan^{-1}\left(\frac{l_{JI}^-}{b_{JI}}\right)+b_{JI}\ln\left[\frac{l_{JI}^-+\sqrt{a_I^2+b_{JI}^2+(l_{JI}^-)^2}}{\sqrt{a_I^2+b_{JI}^2}}\right]. \tag{28}$$

Note that $e^{-r/L}$ can be written as a power series:

$$e^{-r/L}=\sum_{n=0}^{\infty}\frac{(-1)^n}{n!}\left(\frac{r}{L}\right)^n. \tag{29}$$

Using Eq. (29) in Eq. (25) then leads to

$$\Gamma_{,i}=-\sum_{I=1}^{p}\sum_{J=1}^{q}(\zeta_I^0)_i L\Bigg\{e^{-a_I/L}\left[\tan^{-1}\left(\frac{l_{JI}^+}{b_{JI}}\right)-\tan^{-1}\left(\frac{l_{JI}^-}{b_{JI}}\right)\right]$$

$$+\sum_{n=0}^{\infty}\frac{(-1)^{n+1}}{L^n n!}\frac{l_{JI}^+[a_I^2+b_{JI}^2+(l_{JI}^+)^2]^{n/2}}{b_{JI}}\left[1+\frac{(l_{JI}^+)^2}{a_I^2+b_{JI}^2}\right]^{-n/2}F_1\left[\frac{1}{2},-\frac{n}{2},1,\frac{3}{2},-\frac{(l_{JI}^+)^2}{a_I^2+b_{JI}^2},-\frac{(l_{JI}^+)^2}{b_{JI}^2}\right]$$

$$-\sum_{n=0}^{\infty}\frac{(-1)^{n+1}}{L^n n!}\frac{l_{JI}^-[a_I^2+b_{JI}^2+(l_{JI}^-)^2]^{n/2}}{b_{JI}}\left[1+\frac{(l_{JI}^-)^2}{a_I^2+b_{JI}^2}\right]^{-n/2}F_1\left[\frac{1}{2},-\frac{n}{2},1,\frac{3}{2},-\frac{(l_{JI}^-)^2}{a_I^2+b_{JI}^2},-\frac{(l_{JI}^-)^2}{b_{JI}^2}\right]\Bigg\}$$

$$\equiv-\sum_{I=1}^{p}\sum_{J=1}^{q}(\zeta_I^0)_i\Gamma_1^{JI}=-\sum_{I=1}^{p}\sum_{J=1}^{q}(\zeta_I^0)_i[(\Gamma_1^{JI})^+-(\Gamma_1^{JI})^-], \tag{30}$$

where Γ_1^{JI}, $(\Gamma_1^{JI})^+$ and $(\Gamma_1^{JI})^-$ are functions defined by

$$\Gamma_1^{JI} = \Gamma_1^{JI}(a_I,b_{JI},l_{JI}^+,l_{JI}^-) = (\Gamma_1^{JI})^+(a_I,b_{JI},l_{JI}^+) - (\Gamma_1^{JI})^-(a_I,b_{JI},l_{JI}^-),$$

$$(\Gamma_1^{JI})^+ = L\left\{ e^{-a_I/L}\tan^{-1}\left(\frac{l_{JI}^+}{b_{JI}}\right) + \sum_{n=0}^{\infty}\frac{(-1)^{n+1}}{L^n n!}\frac{l_{JI}^+[a_I^2+b_{JI}^2+(l_{JI}^+)^2]^{n/2}}{b_{JI}}\left[1+\frac{(l_{JI}^+)^2}{a_I^2+b_{JI}^2}\right]^{-n/2} F_1\left[\frac{1}{2},-\frac{n}{2},1,\frac{3}{2},-\frac{(l_{JI}^+)^2}{a_I^2+b_{JI}^2},-\frac{(l_{JI}^+)^2}{b_{JI}^2}\right]\right\},$$

$$(\Gamma_1^{JI})^- = L\left\{ e^{-a_I/L}\tan^{-1}\left(\frac{l_{JI}^-}{b_{JI}}\right) + \sum_{n=0}^{\infty}\frac{(-1)^{n+1}}{L^n n!}\frac{l_{JI}^-[a_I^2+b_{JI}^2+(l_{JI}^-)^2]^{n/2}}{b_{JI}}\left[1+\frac{(l_{JI}^-)^2}{a_I^2+b_{JI}^2}\right]^{-n/2} F_1\left[\frac{1}{2},-\frac{n}{2},1,\frac{3}{2},-\frac{(l_{JI}^-)^2}{a_I^2+b_{JI}^2},-\frac{(l_{JI}^-)^2}{b_{JI}^2}\right]\right\}, \tag{31}$$

and F_1 is the first Appell hypergeometric function of two variables given by

$$F_1(a,b,c,d;x,y) = \sum_{m,n=0}^{\infty}\frac{(a)_{m+n}(b)_m(c)_n}{(d)_{m+n}m!n!}x^m y^n, \tag{32}$$

with $(f)_m$ being the Pochhammer symbol representing the following rising factorial:

$$(f)_m = \frac{\Gamma(f+m)}{\Gamma(f)} = f(f+1)(f+2)\cdots(f+m-1). \tag{33}$$

Note that Eqs. (26), (27) and (30) are applicable to both the interior case with $\mathbf{x}$ being inside the polyhedral inclusion (i.e., $\mathbf{x}\in\Omega$) and the exterior case with $\mathbf{x}$ being outside the inclusion (i.e., $\mathbf{x}\notin\Omega$). For the former a_I is a positive value, while for the latter a_I is a negative value. The similarity and difference identified here between the interior and exterior cases can be seen from Fig. 3, where how the duplex in each case is constructed is schematically shown.

It should be mentioned that no attempt is made here to obtain the expressions of the potential functions $\Phi(\mathbf{x})$, $\Lambda(\mathbf{x})$ and $\Gamma(\mathbf{x})$ from Eqs. (26), (27) and (30), since only the second and/or fourth derivatives of these functions are involved in the general expressions of the Eshelby tensor given in Eqs. (9a), (9b) and (9c).

Note that for a smooth function $F(\mathbf{x}) \equiv F(a_I,b_{JI},l_{JI}^+,l_{JI}^-) = F^+(a_I,b_{JI},l_{JI}^+) - F^-(a_I,b_{JI},l_{JI}^-)$ the use of chain rule gives

$$F_{,i} \equiv \frac{\partial F}{\partial x_i} = \frac{\partial F}{\partial a_I}\frac{\partial a_I}{\partial x_i} + \frac{\partial F}{\partial b_{JI}}\frac{\partial b_{JI}}{\partial x_i} + \frac{\partial F^+}{\partial l_{JI}^+}\frac{\partial l_{JI}^+}{\partial x_i} - \frac{\partial F^-}{\partial l_{JI}^-}\frac{\partial l_{JI}^-}{\partial x_i}, \tag{34}$$

where the parameters a_I, b_{JI}, l_{JI}^+, l_{JI}^- are related to $\mathbf{x}$ through

$$a_I = (v_k^+ - x_k)(\zeta_I^0)_k, \tag{35a}$$

$$b_{JI} = (v_k^+ - x_k)(\lambda_{JI}^0)_k, \tag{35b}$$

$$l_{JI}^+ = (v_k^+ - x_k)(\eta_{JI}^0)_k, \tag{35c}$$

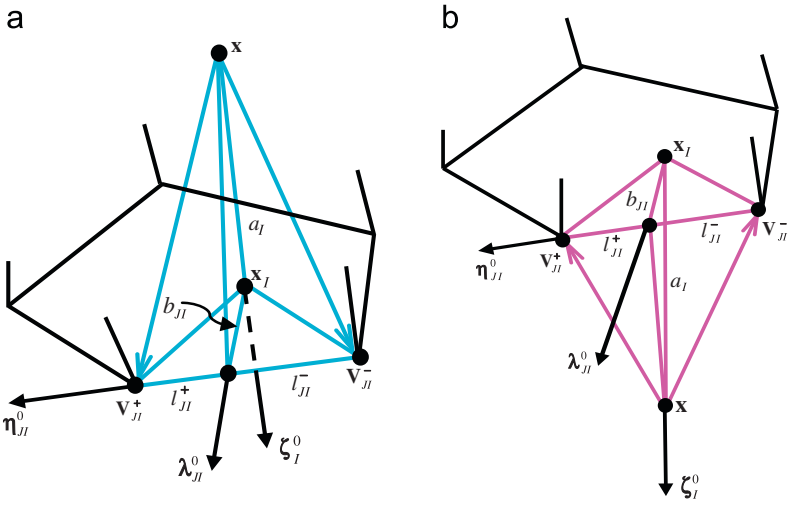

Fig. 3. Duplex and parameters a_I, b_{JI}, l_{JI}^+, l_{JI}^- for (a) $\mathbf{x}\in\Omega$ and (b) $\mathbf{x}\notin\Omega$.

$$l_{JI}^{-}=(v_k^{-}-x_k)(\eta_{JI}^0)_k, \tag{35d}$$

where x_k, v_k^+ and v_k^- are, respectively, the coordinates of the points $\mathbf{x}$, $\mathbf{V}_{JI}^+$ and $\mathbf{V}_{JI}^-$ in the global coordinate system, and $(\zeta_I^0)_k$, $(\lambda_{JI}^0)_k$ and $(\eta_{JI}^0)_k$ are the components of the unit base vectors $\boldsymbol{\zeta}_I^0$, $\boldsymbol{\lambda}_{JI}^0$ and $\boldsymbol{\eta}_{JI}^0$ in the global coordinate system.

It then follows from Eqs. (34), (35a), (35b), (35c) and (35d) that

$$F_{,i}=-\frac{\partial F}{\partial a_I}(\zeta_I^0)_i-\frac{\partial F}{\partial b_{JI}}(\lambda_{JI}^0)_i-\left(\frac{\partial F^+}{\partial l_{JI}^+}-\frac{\partial F^-}{\partial l_{JI}^-}\right)(\eta_{JI}^0)_i, \tag{36a}$$

$$\begin{aligned}
F_{,ijk}=&-\frac{\partial^3 F}{\partial a_I^3}(\zeta_I^0)_i(\zeta_I^0)_j(\zeta_I^0)_k-\frac{\partial^3 F}{\partial b_{JI}^3}(\lambda_{JI}^0)_i(\lambda_{JI}^0)_j(\lambda_{JI}^0)_k-\left[\frac{\partial^3 F^+}{\partial(l_{JI}^+)^3}-\frac{\partial^3 F^-}{\partial(l_{JI}^-)^3}\right](\eta_{JI}^0)_i(\eta_{JI}^0)_j(\eta_{JI}^0)_k\\
&-\frac{\partial^3 F}{\partial a_I^2\partial b_{JI}}[(\lambda_{JI}^0)_i(\zeta_I^0)_j(\zeta_I^0)_k+(\zeta_I^0)_i(\lambda_{JI}^0)_j(\zeta_I^0)_k+(\zeta_I^0)_i(\zeta_I^0)_j(\lambda_{JI}^0)_k]-\left[\frac{\partial^3 F^+}{\partial a_I^2\partial l_{JI}^+}-\frac{\partial^3 F^-}{\partial a_I^2\partial l_{JI}^-}\right][(\eta_{JI}^0)_i(\zeta_I^0)_j(\zeta_I^0)_k+(\zeta_I^0)_i(\eta_{JI}^0)_j(\zeta_I^0)_k\\
&+(\zeta_I^0)_i(\zeta_I^0)_j(\eta_{JI}^0)_k]-\frac{\partial^3 F}{\partial a_I\partial b_{JI}^2}[(\zeta_I^0)_i(\lambda_{JI}^0)_j(\lambda_{JI}^0)_k+(\lambda_{JI}^0)_i(\zeta_I^0)_j(\lambda_{JI}^0)_k+(\lambda_{JI}^0)_i(\lambda_{JI}^0)_j(\zeta_I^0)_k]-\left(\frac{\partial^3 F^+}{\partial b_{JI}^2\partial l_{JI}^+}-\frac{\partial^3 F^-}{\partial b_{JI}^2\partial l_{JI}^-}\right)[(\eta_{JI}^0)_i(\lambda_{JI}^0)_j(\lambda_{JI}^0)_k\\
&+(\lambda_{JI}^0)_i(\eta_{JI}^0)_j(\lambda_{JI}^0)_k+(\lambda_{JI}^0)_i(\lambda_{JI}^0)_j(\eta_{JI}^0)_k]-\left[\frac{\partial^3 F^+}{\partial a_I\partial(l_{JI}^+)^2}-\frac{\partial^3 F^-}{\partial a_I\partial(l_{JI}^-)^2}\right][(\zeta_I^0)_i(\eta_{JI}^0)_j(\eta_{JI}^0)_k+(\eta_{JI}^0)_i(\zeta_I^0)_j(\eta_{JI}^0)_k+(\eta_{JI}^0)_i(\eta_{JI}^0)_j(\zeta_I^0)_k]\\
&-\left[\frac{\partial^3 F^+}{\partial b_{JI}\partial(l_{JI}^+)^2}-\frac{\partial^3 F^-}{\partial b_{JI}\partial(l_{JI}^-)^2}\right][(\lambda_{JI}^0)_i(\eta_{JI}^0)_j(\eta_{JI}^0)_k+(\eta_{JI}^0)_i(\lambda_{JI}^0)_j(\eta_{JI}^0)_k+(\eta_{JI}^0)_i(\eta_{JI}^0)_j(\lambda_{JI}^0)_k]\\
&-\left(\frac{\partial^3 F^+}{\partial a_I\partial b_{JI}\partial l_{JI}^+}-\frac{\partial^3 F^-}{\partial a_I\partial b_{JI}\partial l_{JI}^-}\right)[(\zeta_I^0)_i(\lambda_{JI}^0)_j(\eta_{JI}^0)_k+(\zeta_I^0)_i(\eta_{JI}^0)_j(\lambda_{JI}^0)_k+(\lambda_{JI}^0)_i(\zeta_I^0)_j(\eta_{JI}^0)_k\\
&+(\lambda_{JI}^0)_i(\eta_{JI}^0)_j(\zeta_I^0)_k+(\eta_{JI}^0)_i(\zeta_I^0)_j(\lambda_{JI}^0)_k+(\eta_{JI}^0)_i(\lambda_{JI}^0)_j(\zeta_I^0)_k].
\end{aligned} \tag{36b}$$

Using Eqs. (26), (27), (30), (36a) and (36b) in Eqs. (9b) and (9c) will lead to the final expressions of the Eshelby tensor for the p-faced polyhedral inclusion as

$$\begin{aligned}
S_{ijkl}^C=&\frac{1}{8\pi(1-\nu)}\sum_{I=1}^{p}\sum_{J=1}^{q}[(S_1^C)_{JI}(\zeta_I^0)_i(\zeta_I^0)_j\delta_{kl}+(S_2^C)_{JI}[(\zeta_I^0)_i(\zeta_I^0)_k\delta_{jl}+(\zeta_I^0)_i(\zeta_I^0)_l\delta_{jk}]\\
&+(S_3^C)_{JI}[(\zeta_I^0)_k(\zeta_I^0)_j\delta_{il}+(\zeta_I^0)_l(\zeta_I^0)_j\delta_{ik}]+(S_4^C)_{JI}(\zeta_I^0)_i(\lambda_{JI}^0)_j\delta_{kl}+(S_5^C)_{JI}[(\zeta_I^0)_i(\lambda_{JI}^0)_k\delta_{jl}+(\zeta_I^0)_i(\lambda_{JI}^0)_l\delta_{jk}]\\
&+(S_6^C)_{JI}[(\lambda_{JI}^0)_k(\zeta_I^0)_j\delta_{il}+(\lambda_{JI}^0)_l(\zeta_I^0)_j\delta_{ik}]+(S_7^C)_{JI}(\zeta_I^0)_i(\eta_{JI}^0)_j\delta_{kl}+(S_8^C)_{JI}[(\zeta_I^0)_i(\eta_{JI}^0)_k\delta_{jl}+(\zeta_I^0)_i(\eta_{JI}^0)_l\delta_{jk}]\\
&+(S_9^C)_{JI}[(\eta_{JI}^0)_k(\zeta_I^0)_j\delta_{il}+(\eta_{JI}^0)_l(\zeta_I^0)_j\delta_{ik}]+(S_{10}^C)_{JI}[(\zeta_I^0)_i(\lambda_{JI}^0)_j(\zeta_I^0)_k(\zeta_I^0)_l+(\zeta_I^0)_i(\zeta_I^0)_j(\lambda_{JI}^0)_k(\zeta_I^0)_l+(\zeta_I^0)_i(\zeta_I^0)_j(\zeta_I^0)_k(\lambda_{JI}^0)_l]\\
&+(S_{11}^C)_{JI}[(\zeta_I^0)_i(\eta_{JI}^0)_j(\zeta_I^0)_k(\zeta_I^0)_l+(\zeta_I^0)_i(\zeta_I^0)_j(\eta_{JI}^0)_k(\zeta_I^0)_l+(\zeta_I^0)_i(\zeta_I^0)_j(\zeta_I^0)_k(\eta_{JI}^0)_l]+(S_{12}^C)_{JI}[(\zeta_I^0)_i(\zeta_I^0)_j(\lambda_{JI}^0)_k(\lambda_{JI}^0)_l\\
&+(\zeta_I^0)_i(\lambda_{JI}^0)_j(\zeta_I^0)_k(\lambda_{JI}^0)_l+(\zeta_I^0)_i(\lambda_{JI}^0)_j(\lambda_{JI}^0)_k(\zeta_I^0)_l]+(S_{13}^C)_{JI}[(\zeta_I^0)_i(\zeta_I^0)_j(\eta_{JI}^0)_k(\eta_{JI}^0)_l+(\zeta_I^0)_i(\eta_{JI}^0)_j(\zeta_I^0)_k(\eta_{JI}^0)_l+(\zeta_I^0)_i(\eta_{JI}^0)_j(\eta_{JI}^0)_k(\zeta_I^0)_l]\\
&+(S_{14}^C)_{JI}[(\zeta_I^0)_i(\lambda_{JI}^0)_j(\eta_{JI}^0)_k(\eta_{JI}^0)_l+(\zeta_I^0)_i(\eta_{JI}^0)_j(\lambda_{JI}^0)_k(\eta_{JI}^0)_l+(\zeta_I^0)_i(\eta_{JI}^0)_j(\eta_{JI}^0)_k(\lambda_{JI}^0)_l]+(S_{15}^C)_{JI}[(\zeta_I^0)_i(\eta_{JI}^0)_j(\lambda_{JI}^0)_k(\lambda_{JI}^0)_l\\
&+(\zeta_I^0)_i(\lambda_{JI}^0)_j(\eta_{JI}^0)_k(\lambda_{JI}^0)_l+(\zeta_I^0)_i(\lambda_{JI}^0)_j(\lambda_{JI}^0)_k(\eta_{JI}^0)_l]+(S_{16}^C)_{JI}[(\zeta_I^0)_i(\zeta_I^0)_j(\lambda_{JI}^0)_k(\eta_{JI}^0)_l+(\zeta_I^0)_i(\zeta_I^0)_j(\eta_{JI}^0)_k(\lambda_{JI}^0)_l+(\zeta_I^0)_i(\lambda_{JI}^0)_j(\eta_{JI}^0)_k(\zeta_I^0)_l\\
&+(\zeta_I^0)_i(\lambda_{JI}^0)_j(\zeta_I^0)_k(\eta_{JI}^0)_l+(\zeta_I^0)_i(\eta_{JI}^0)_j(\zeta_I^0)_k(\lambda_{JI}^0)_l+(\zeta_I^0)_i(\eta_{JI}^0)_j(\lambda_{JI}^0)_k(\zeta_I^0)_l]],
\end{aligned} \tag{37a}$$

where

$$\begin{aligned}
&(S_1^C)_{JI}=\frac{1}{3}\frac{\partial^3\Phi_1^{JI}}{\partial a_I^3}-2\nu\frac{\partial\Lambda_1^{JI}}{\partial a_I},\quad (S_2^C)_{JI}=\frac{1}{3}\frac{\partial^3\Phi_1^{JI}}{\partial a_I^3}-(1-\nu)\frac{\partial\Lambda_1^{JI}}{\partial a_I},\quad (S_3^C)_{JI}=-(1-\nu)\frac{\partial\Lambda_1^{JI}}{\partial a_I},\quad (S_4^C)_{JI}=\frac{1}{3}\frac{\partial^3\Phi_1^{JI}}{\partial b_{JI}^3}-2\nu\frac{\partial\Lambda_1^{JI}}{\partial b_{JI}},\\
&(S_5^C)_{JI}=\frac{1}{3}\frac{\partial^3\Phi_1^{JI}}{\partial b_{JI}^3}-(1-\nu)\frac{\partial\Lambda_1^{JI}}{\partial b_{JI}},\quad (S_6^C)_{JI}=-(1-\nu)\frac{\partial\Lambda_1^{JI}}{\partial b_{JI}},\quad (S_7^C)_{JI}=\frac{1}{3}\left[\frac{\partial^3(\Phi_1^{JI})^+}{\partial(l_{JI}^+)^3}-\frac{\partial^3(\Phi_1^{JI})^-}{\partial(l_{JI}^-)^3}\right]-2\nu\left[\frac{\partial(\Lambda_1^{JI})^+}{\partial l_{JI}^+}-\frac{\partial(\Lambda_1^{JI})^-}{\partial l_{JI}^-}\right],\\
&(S_8^C)_{JI}=\frac{1}{3}\left[\frac{\partial^3(\Phi_1^{JI})^+}{\partial(l_{JI}^+)^3}-\frac{\partial^3(\Phi_1^{JI})^-}{\partial(l_{JI}^-)^3}\right]-(1-\nu)\left[\frac{\partial(\Lambda_1^{JI})^+}{\partial l_{JI}^+}-\frac{\partial(\Lambda_1^{JI})^-}{\partial l_{JI}^-}\right],\quad (S_9^C)_{JI}=-(1-\nu)\left[\frac{\partial(\Lambda_1^{JI})^+}{\partial l_{JI}^+}-\frac{\partial(\Lambda_1^{JI})^-}{\partial l_{JI}^-}\right],\\
&(S_{10}^C)_{JI}=\frac{\partial^3\Phi_1^{JI}}{\partial a_I^2\partial b_{JI}}-\frac{1}{3}\frac{\partial^3\Phi_1^{JI}}{\partial b_{JI}^3},\quad (S_{11}^C)_{JI}=\frac{\partial^3(\Phi_1^{JI})^+}{\partial a_I^2\partial l_{JI}^+}-\frac{\partial^3(\Phi_1^{JI})^-}{\partial a_I^2\partial l_{JI}^-}-\frac{1}{3}\left[\frac{\partial^3(\Phi_1^{JI})^+}{\partial(l_{JI}^+)^3}-\frac{\partial^3(\Phi_1^{JI})^-}{\partial(l_{JI}^-)^3}\right],\quad (S_{12}^C)_{JI}=\frac{\partial^3\Phi_1^{JI}}{\partial b_{JI}^2\partial a_I}-\frac{1}{3}\frac{\partial^3\Phi_1^{JI}}{\partial a_I^3},\\
&(S_{13}^C)_{JI}=\left[\frac{\partial^3(\Phi_1^{JI})^+}{\partial(l_{JI}^+)^2\partial a_I}-\frac{\partial^3(\Phi_1^{JI})^-}{\partial(l_{JI}^-)^2\partial a_I}\right]-\frac{1}{3}\frac{\partial^3\Phi_1^{JI}}{\partial a_I^3},\quad (S_{14}^C)_{JI}=\left[\frac{\partial^3(\Phi_1^{JI})^+}{\partial(l_{JI}^+)^2\partial b_{JI}}-\frac{\partial^3(\Phi_1^{JI})^-}{\partial(l_{JI}^-)^2\partial b_{JI}}\right]-\frac{1}{3}\frac{\partial^3\Phi_1^{JI}}{\partial b_{JI}^3},\\
&(S_{15}^C)_{JI}=\frac{\partial^3(\Phi_1^{JI})^+}{\partial b_{JI}^2\partial l_{JI}^+}-\frac{\partial^3(\Phi_1^{JI})^-}{\partial b_{JI}^2\partial l_{JI}^-}-\frac{1}{3}\left[\frac{\partial^3(\Phi_1^{JI})^+}{\partial(l_{JI}^+)^3}-\frac{\partial^3(\Phi_1^{JI})^-}{\partial(l_{JI}^-)^3}\right],\quad (S_{16}^C)_{JI}=\frac{\partial^3(\Phi_1^{JI})^+}{\partial a_I\partial b_{JI}\partial l_{JI}^+}-\frac{\partial^3(\Phi_1^{JI})^-}{\partial a_I\partial b_{JI}\partial l_{JI}^-},
\end{aligned} \tag{37b}$$

and

$$
\begin{aligned}
S^G_{ijkl} = \frac{1}{8\pi(1-\nu)}\sum_{J=1}^{q}\sum_{I=1}^{p}\{&(S^G_1)_{JI}(\zeta^0_I)_i(\zeta^0_I)_j\delta_{kl}+(S^G_2)_{JI}[(\zeta^0_I)_i(\zeta^0_I)_k\delta_{jl}+(\zeta^0_I)_i(\zeta^0_I)_l\delta_{jk}]+(S^G_3)_{JI}[(\zeta^0_I)_k(\zeta^0_I)_j\delta_{il}+(\zeta^0_I)_l(\zeta^0_I)_j\delta_{ik}]\\
&+(S^G_4)_{JI}(\zeta^0_I)_i(\lambda^0_{JI})_j\delta_{kl}+(S^G_5)_{JI}[(\zeta^0_I)_i(\lambda^0_{JI})_k\delta_{jl}+(\zeta^0_I)_i(\lambda^0_{JI})_l\delta_{jk}]+(S^G_6)_{JI}[(\lambda^0_{JI})_k(\zeta^0_I)_j\delta_{il}+(\lambda^0_{JI})_l(\zeta^0_I)_j\delta_{ik}]\\
&+(S^G_7)_{JI}(\zeta^0_I)_i(\eta^0_{JI})_j\delta_{kl}+(S^G_8)_{JI}[(\zeta^0_I)_i(\eta^0_{JI})_k\delta_{jl}+(\zeta^0_I)_i(\eta^0_{JI})_l\delta_{jk}]+(S^G_9)_{JI}[(\eta^0_{JI})_k(\zeta^0_I)_j\delta_{il}+(\eta^0_{JI})_l(\zeta^0_I)_j\delta_{ik}]\\
&+(S^G_{10})_{JI}[(\zeta^0_I)_i(\lambda^0_{JI})_j(\zeta^0_I)_k(\zeta^0_I)_l+(\zeta^0_I)_i(\zeta^0_I)_j(\lambda^0_{JI})_k(\zeta^0_I)_l+(\zeta^0_I)_i(\zeta^0_I)_j(\zeta^0_I)_k(\lambda^0_{JI})_l]+(S^G_{11})_{JI}[(\zeta^0_I)_i(\eta^0_{JI})_j(\zeta^0_I)_k(\zeta^0_I)_l\\
&+(\zeta^0_I)_i(\zeta^0_I)_j(\eta^0_{JI})_k(\zeta^0_I)_l+(\zeta^0_I)_i(\zeta^0_I)_j(\zeta^0_I)_k(\eta^0_{JI})_l]+(S^G_{12})_{JI}[(\zeta^0_I)_i(\zeta^0_I)_j(\lambda^0_{JI})_k(\lambda^0_{JI})_l+(\zeta^0_I)_i(\lambda^0_{JI})_j(\zeta^0_I)_k(\lambda^0_{JI})_l+(\zeta^0_I)_i(\lambda^0_{JI})_j(\lambda^0_{JI})_k(\zeta^0_I)_l]\\
&+(S^G_{13})_{JI}[(\zeta^0_I)_i(\zeta^0_I)_j(\eta^0_{JI})_k(\eta^0_{JI})_l+(\zeta^0_I)_i(\eta^0_{JI})_j(\zeta^0_I)_k(\eta^0_{JI})_l+(\zeta^0_I)_i(\eta^0_{JI})_j(\eta^0_{JI})_k(\zeta^0_I)_l]+(S^G_{14})_{JI}[(\zeta^0_I)_i(\lambda^0_{JI})_j(\eta^0_{JI})_k(\eta^0_{JI})_l\\
&+(\zeta^0_I)_i(\eta^0_{JI})_j(\lambda^0_{JI})_k(\eta^0_{JI})_l+(\zeta^0_I)_i(\eta^0_{JI})_j(\eta^0_{JI})_k(\lambda^0_{JI})_l]+(S^G_{15})_{JI}[(\zeta^0_I)_i(\eta^0_{JI})_j(\lambda^0_{JI})_k(\lambda^0_{JI})_l+(\zeta^0_I)_i(\lambda^0_{JI})_j(\eta^0_{JI})_k(\lambda^0_{JI})_l+(\zeta^0_I)_i(\lambda^0_{JI})_j(\lambda^0_{JI})_k(\eta^0_{JI})_l]\\
&+(S^G_{16})_{JI}[(\zeta^0_I)_i(\zeta^0_I)_j(\lambda^0_{JI})_k(\eta^0_{JI})_l+(\zeta^0_I)_i(\zeta^0_I)_j(\eta^0_{JI})_k(\lambda^0_{JI})_l+(\zeta^0_I)_i(\lambda^0_{JI})_j(\eta^0_{JI})_k(\zeta^0_I)_l+(\zeta^0_I)_i(\lambda^0_{JI})_j(\zeta^0_I)_k(\eta^0_{JI})_l\\
&+(\zeta^0_I)_i(\eta^0_{JI})_j(\zeta^0_I)_k(\lambda^0_{JI})_l+(\zeta^0_I)_i(\eta^0_{JI})_j(\lambda^0_{JI})_k(\zeta^0_I)_l]\},
\end{aligned}
\tag{37c}
$$

where

$$
(S^G_1)_{JI}=\frac{2L^2}{3}\frac{\partial^3(\Lambda^{JI}_1-\Gamma^{JI}_1)}{\partial a_I^3}+\frac{4\nu(1-\nu)}{(1-2\nu)}\frac{\partial\Gamma^{JI}_1}{\partial a_I}+\frac{2\nu L^2}{(1-2\nu)}\left\{\frac{\partial^3(\Lambda^{JI}_1-\Gamma^{JI}_1)}{\partial a_I^3}+\frac{\partial^3(\Lambda^{JI}_1-\Gamma^{JI}_1)}{\partial a_I\partial b_{JI}^2}+\frac{\partial^3[(\Lambda^{JI}_1)^+-(\Gamma^{JI}_1)^+]}{\partial a_I\partial(l^+_{JI})^2}-\frac{\partial^3[(\Lambda^{JI}_1)^--(\Gamma^{JI}_1)^-]}{\partial a_I\partial(l^-_{JI})^2}\right\},
$$

$$
(S^G_2)_{JI}=\frac{2L^2}{3}\frac{\partial^3(\Lambda^{JI}_1-\Gamma^{JI}_1)}{\partial a_I^3}+(1-\nu)\frac{\partial\Gamma^{JI}_1}{\partial a_I},\quad (S^G_3)_{JI}=(1-\nu)\frac{\partial\Gamma^{JI}_1}{\partial a_I},
$$

$$
(S^G_4)_{JI}=\frac{2L^2}{3}\frac{\partial^3(\Lambda^{JI}_1-\Gamma^{JI}_1)}{\partial b_{JI}^3}+\frac{4\nu(1-\nu)}{(1-2\nu)}\frac{\partial\Gamma^{JI}_1}{\partial b_{JI}}+\frac{2\nu L^2}{(1-2\nu)}\left\{\frac{\partial^3(\Lambda^{JI}_1-\Gamma^{JI}_1)}{\partial a_I^2\partial b_{JI}}+\frac{\partial^3(\Lambda^{JI}_1-\Gamma^{JI}_1)}{\partial b_{JI}^3}+\frac{\partial^3[(\Lambda^{JI}_1)^+-(\Gamma^{JI}_1)^+]}{\partial b_{JI}\partial(l^+_{JI})^2}-\frac{\partial^3[(\Lambda^{JI}_1)^--(\Gamma^{JI}_1)^-]}{\partial b_{JI}\partial(l^-_{JI})^2}\right\},
$$

$$
(S^G_5)_{JI}=\frac{2L^2}{3}\frac{\partial^3(\Lambda^{JI}_1-\Gamma^{JI}_1)}{\partial b_{JI}^3}+(1-\nu)\frac{\partial\Gamma^{JI}_1}{\partial b_{JI}},\quad (S^G_6)_{JI}=(1-\nu)\frac{\partial\Gamma^{JI}_1}{\partial b_{JI}},
$$

$$
\begin{aligned}
(S^G_7)_{JI}=&\frac{2L^2}{3}\left\{\frac{\partial^3[(\Lambda^{JI}_1)^+-(\Gamma^{JI}_1)^+]}{\partial(l^+_{JI})^3}-\frac{\partial^3[(\Lambda^{JI}_1)^--(\Gamma^{JI}_1)^-]}{\partial(l^-_{JI})^3}\right\}+\frac{4\nu(1-\nu)}{(1-2\nu)}\left[\frac{\partial(\Gamma^{JI}_1)^+}{\partial l^+_{JI}}-\frac{\partial(\Gamma^{JI}_1)^-}{\partial l^-_{JI}}\right]\\
&+\frac{2\nu L^2}{(1-2\nu)}\left\{\frac{\partial^3[(\Lambda^{JI}_1)^+-(\Gamma^{JI}_1)^+]}{\partial a_I^2\partial l^+_{JI}}-\frac{\partial^3[(\Lambda^{JI}_1)^--(\Gamma^{JI}_1)^-]}{\partial a_I^2\partial l^-_{JI}}+\frac{\partial^3[(\Lambda^{JI}_1)^+-(\Gamma^{JI}_1)^+]}{\partial b_{JI}^2\partial l^+_{JI}}-\frac{\partial^3[(\Lambda^{JI}_1)^--(\Gamma^{JI}_1)^-]}{\partial b_{JI}^2\partial l^-_{JI}}\right.\\
&\left.+\frac{\partial^3[(\Lambda^{JI}_1)^+-(\Gamma^{JI}_1)^+]}{\partial(l^+_{JI})^3}-\frac{\partial^3[(\Lambda^{JI}_1)^--(\Gamma^{JI}_1)^-]}{\partial(l^-_{JI})^3}\right\},
\end{aligned}
$$

$$
(S^G_8)_{JI}=\frac{2L^2}{3}\left\{\frac{\partial^3[(\Lambda^{JI}_1)^+-(\Gamma^{JI}_1)^+]}{\partial(l^+_{JI})^3}-\frac{\partial^3[(\Lambda^{JI}_1)^--(\Gamma^{JI}_1)^-]}{\partial(l^-_{JI})^3}\right\}+(1-\nu)\left[\frac{\partial(\Gamma^{JI}_1)^+}{\partial l^+_{JI}}-\frac{\partial(\Gamma^{JI}_1)^-}{\partial l^-_{JI}}\right],
$$

$$
(S^G_9)_{JI}=(1-\nu)\left[\frac{\partial(\Gamma^{JI}_1)^+}{\partial l^+_{JI}}-\frac{\partial(\Gamma^{JI}_1)^-}{\partial l^-_{JI}}\right],\quad (S^G_{10})_{JI}=2L^2\left[\frac{\partial^3(\Lambda^{JI}_1-\Gamma^{JI}_1)}{\partial a_I^2\partial b_{JI}}-\frac{1}{3}\frac{\partial^3(\Lambda^{JI}_1-\Gamma^{JI}_1)}{\partial b_{JI}^3}\right],
$$

$$
(S^G_{11})_{JI}=2L^2\left\{\frac{\partial^3[(\Lambda^{JI}_1)^+-(\Gamma^{JI}_1)^+]}{\partial a_I^2\partial l^+_{JI}}-\frac{\partial^3[(\Lambda^{JI}_1)^--(\Gamma^{JI}_1)^-]}{\partial a_I^2\partial l^-_{JI}}-\frac{1}{3}\frac{\partial^3[(\Lambda^{JI}_1)^+-(\Gamma^{JI}_1)^+]}{\partial(l^+_{JI})^3}+\frac{1}{3}\frac{\partial^3[(\Lambda^{JI}_1)^--(\Gamma^{JI}_1)^-]}{\partial(l^-_{JI})^3}\right\},
$$

$$
(S^G_{12})_{JI}=2L^2\left[\frac{\partial^3(\Lambda^{JI}_1-\Gamma^{JI}_1)}{\partial b_{JI}^2\partial a_I}-\frac{1}{3}\frac{\partial^3(\Lambda^{JI}_1-\Gamma^{JI}_1)}{\partial a_I^3}\right],\quad (S^G_{13})_{JI}=2L^2\left\{\frac{\partial^3[(\Lambda^{JI}_1)^+-(\Gamma^{JI}_1)^+]}{\partial a_I\partial(l^+_{JI})^2}-\frac{\partial^3[(\Lambda^{JI}_1)^--(\Gamma^{JI}_1)^-]}{\partial a_I\partial(l^-_{JI})^2}-\frac{1}{3}\frac{\partial^3(\Lambda^{JI}_1-\Gamma^{JI}_1)}{\partial a_I^3}\right\},
$$

$$
(S^G_{14})_{JI}=2L^2\left\{\frac{\partial^3[(\Lambda^{JI}_1)^+-(\Gamma^{JI}_1)^+]}{\partial b_{JI}\partial(l^+_{JI})^2}-\frac{\partial^3[(\Lambda^{JI}_1)^--(\Gamma^{JI}_1)^-]}{\partial b_{JI}\partial(l^-_{JI})^2}-\frac{1}{3}\frac{\partial^3(\Lambda^{JI}_1-\Gamma^{JI}_1)}{\partial b_{JI}^3}\right\},
$$

$$
(S^G_{15})_{JI}=2L^2\left\{\frac{\partial^3[(\Lambda^{JI}_1)^+-(\Gamma^{JI}_1)^+]}{\partial b_{JI}^2\partial l^+_{JI}}-\frac{\partial^3[(\Lambda^{JI}_1)^--(\Gamma^{JI}_1)^-]}{\partial b_{JI}^2\partial l^-_{JI}}-\frac{1}{3}\frac{\partial^3[(\Lambda^{JI}_1)^+-(\Gamma^{JI}_1)^+]}{\partial(l^+_{JI})^3}+\frac{1}{3}\frac{\partial^3[(\Lambda^{JI}_1)^--(\Gamma^{JI}_1)^-]}{\partial(l^-_{JI})^3}\right\},
$$

$$
(S^G_{16})_{JI}=2L^2\left\{\left[\frac{\partial^3[(\Lambda^{JI}_1)^+-(\Gamma^{JI}_1)^+]}{\partial a_I\partial b_{JI}\partial l^+_{JI}}-\frac{\partial^3[(\Lambda^{JI}_1)^--(\Gamma^{JI}_1)^-]}{\partial a_I\partial b_{JI}\partial l^-_{JI}}\right]\right\}.
\tag{37d}
$$

In Eqs. (37b) and (37d), Φ^{JI}_1, $(\Phi^{JI}_1)^+$, $(\Phi^{JI}_1)^-$, Λ^{JI}_1, $(\Lambda^{JI}_1)^+$, $(\Lambda^{JI}_1)^-$, Γ^{JI}_1, $(\Gamma^{JI}_1)^+$ and $(\Gamma^{JI}_1)^-$ are defined in Eqs. (28) and (31).

It should be mentioned that the classical part S^C_{ijkl} in Eqs. (37a) and (37b) depends only on Poisson's ratio ν and cannot account for the inclusion size effect, noting that Φ^{JI}_1, $(\Phi^{JI}_1)^+$, $(\Phi^{JI}_1)^-$, Λ^{JI}_1, $(\Lambda^{JI}_1)^+$ and $(\Lambda^{JI}_1)^-$ involved in Eq. (37b) do not contain the material length scale parameter L (see Eq. (28)). However, the gradient part S^G_{ijkl} in Eqs. (37c) and (37d) can capture the inclusion size effect, since Eqs. (37c) and (37d) as well as the expressions of Γ^{JI}_1, $(\Gamma^{JI}_1)^+$ and $(\Gamma^{JI}_1)^-$ (see Eq. (31)) contain the

parameter L in addition to Poisson's ratio ν. Clearly, when $L=0$ (i.e., in the absence of the strain gradient effect), $S^G_{ijkl} \equiv 0$ according to Eqs. (37c), (37d) and (31), thereby resulting in $S_{ijkl} = S^C_{ijkl}$ from Eq. (9a). That is, the SSGET-based Eshelby tensor reduces to its counterpart based on classical elasticity when the strain gradient effect is not considered. Also, it is seen that the expressions of the classical elasticity-based Eshelby tensor in Eqs. (37a), (37b) and (28) derived here are more compact than those given in Nozaki and Taya (2001).

The expressions of the Eshelby tensor S_{ijkl} in Eqs. (9a), (37a), (37b), (37c) and (37d) are derived for a p-faced polyhedral inclusion of arbitrary shape. For simple-shape inclusions, more explicit expressions can be obtained for S_{ijkl}.

3.2. Averaged Eshelby tensor

The volume average of the position-dependent Eshelby tensor, $\overline{S}_{ijkl}$, is given by

$$\overline{S}_{ijkl} = \frac{1}{V_\Omega} \sum_{M=1}^{p} \sum_{N=1}^{n} \sum_{I=1}^{p} \sum_{J=1}^{q} \iiint_{\Omega_{NM}} (S_{NM})_{ijkl}(a_I, b_{JI}, l^+_{JI}, l^-_{JI}) dV, \tag{38}$$

where $(S_{NM})_{ijkl}$ is the Eshelby tensor at point $\mathbf{x}$ inside Ω_{NM} presented in Eqs. (9a), (37a), (37b), (37c) and (37d), V_Ω is the volume of the polyhedral inclusion Ω, Ω_{NM} is the region occupied by the duplex formed by the origin (point $\mathbf{O}$) of the global coordinate system, the projection of point $\mathbf{O}$ onto the Mth polygonal surface (i.e., $\mathbf{O}_M$) and two vertices on the Nth edge of the Mth surface (i.e., $\mathbf{V}^+_{NM}$ and $\mathbf{V}^-_{NM}$), and n is the number of edges on the Mth surface. Note that this duplex Ω_{NM} is different from that formed by point $\mathbf{x}$, its projection onto the Ith polygonal surface (i.e., $\mathbf{x}_I$) and two vertices on the Jth edge of the Ith surface (i.e., $\mathbf{V}^+_{JI}$ and $\mathbf{V}^-_{JI}$), as shown in Fig. 4.

For the NMth duplex Ω_{NM} originated from point $\mathbf{O}$, the local Cartesian coordinate system $(\lambda_{NM}, \eta_{NM}, \zeta_M)$ can be chosen in a way similar to what was done earlier (see Fig. 2). Then, the coordinates of the vertices of the duplex Ω_{JI} on the Jth edge of the Ith surface and of an arbitrary point $\mathbf{x}$ within the NMth duplex Ω_{NM} in the $(\lambda_{NM}, \eta_{NM}, \zeta_M)$ local coordinate system can be identified as $(v_1^{JINM+},\ v_2^{JINM+},\ v_3^{JINM+})$, $(v_1^{JINM-},\ v_2^{JINM-},\ v_3^{JINM-})$ and $(x_1^{JINM},\ x_2^{JINM},\ x_3^{JINM})$, respectively. Also, the base vectors $\boldsymbol{\lambda}^0_{JI}$, $\boldsymbol{\eta}^0_{JI}$ and $\boldsymbol{\zeta}^0_I$ of the local coordinate system attached to the duplex Ω_{JI} originated at $\mathbf{x}$ can be expressed in terms of the base vectors $\boldsymbol{\lambda}^0_{NM}$, $\boldsymbol{\eta}^0_{NM}$ and $\boldsymbol{\zeta}^0_M$. It then follows that the parameters for the duplex Ω_{JI} can be determined as

$$a_I = (v_k^{JINM+} - x_k^{JINM})(\zeta^0_I)^{NM}_k = (v_k^{JINM-} - x_k^{JINM})(\zeta^0_I)^{NM}_k, \tag{39a}$$

$$b_{JI} = (v_k^{JINM+} - x_k^{JINM})(\lambda^0_{JI})^{NM}_k = (v_k^{JINM-} - x_k^{JINM})(\lambda^0_{JI})^{NM}_k, \tag{39b}$$

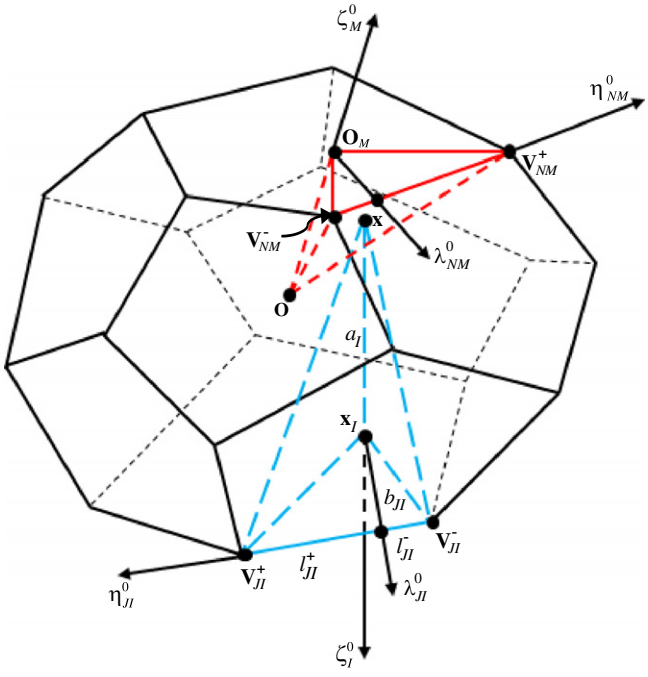

Fig. 4. Duplexes and the corresponding local coordinate systems constructed from an arbitrary point $\mathbf{x}$ and from the origin $\mathbf{O}$ of the global coordinate system, respectively.

$$l_{JI}^{+} = (v_k^{JINM+} - x_k^{JINM})(\eta_{JI}^0)_k^{NM}, \tag{39c}$$

$$l_{JI}^{-} = (v_k^{JINM-} - x_k^{JINM})(\eta_{JI}^0)_k^{NM}, \tag{39d}$$

where $(\lambda_{JI}^0)_k^{NM}$, $(\eta_{JI}^0)_k^{NM}$ and $(\zeta_I^0)_k^{NM}$ represent, respectively, the kth components of the unit vectors $\boldsymbol{\lambda}_{JI}^0$, $\boldsymbol{\eta}_{JI}^0$ and $\boldsymbol{\zeta}_I^0$ in the local coordinate system (λ_{NM}, η_{NM}, ζ_M) with the base vectors $\boldsymbol{\lambda}_{NM}^0$, $\boldsymbol{\eta}_{NM}^0$ and $\boldsymbol{\zeta}_M^0$.

Using Eqs. (39a), (39b), (39c) and (39d) in Eq. (38) yields

$$\overline{S}_{ijkl} = \frac{1}{V_\Omega}\sum_{M=1}^{p}\sum_{N=1}^{n}\sum_{I=1}^{p}\sum_{J=1}^{q}\iiint_{\Omega_{NM}} (S_{NM})_{ijkl}[a_I(\lambda_{NM},\eta_{NM},\zeta_M),\, b_{JI}(\lambda_{NM},\eta_{NM},\zeta_M),\, l_{JI}^{+}(\lambda_{NM},\eta_{NM},\zeta_M),\, l_{JI}^{-}(\lambda_{NM},\eta_{NM},\zeta_M)]d\lambda_{NM}d\eta_{NM}d\zeta_M. \tag{40}$$

This general formula can be used for a polyhedral inclusion of arbitrary shape.

For a polyhedral inclusion that is symmetric about the global coordinate axes x_1, x_2 and x_3, only one eighth of the inclusion needs to be considered and the global coordinate system can be used in all computations. The one-eighth polyhedral domain can be divided into several sub-polyhedra with their top and bottom surfaces parallel to the x_1x_2-plane, and the volume integral over each sub-domain can be evaluated by direct integration using the global coordinate system. Also, only the global coordinates of all vertices need to be determined, and the unit vectors $\boldsymbol{\lambda}_{JI}^0$, $\boldsymbol{\eta}_{JI}^0$ and $\boldsymbol{\zeta}_I^0$ in the local coordinate system can be expressed in terms of the base vectors (i.e., $\mathbf{e}_1$, $\mathbf{e}_2$, $\mathbf{e}_3$) in the global coordinate system. As a result, Eq. (40) can be simplified to

$$\overline{S}_{ijkl} = \frac{8}{V_\Omega}\sum_{T=1}^{t}\sum_{I=1}^{p}\sum_{J=1}^{q}\iiint_{\Omega_T} (S_T)_{ijkl}[a_I(x_1,x_2,x_3),\, b_{JI}(x_1,x_2,x_3),\, l_{JI}^{+}(x_1,x_2,x_3),\, l_{JI}^{-}(x_1,x_2,x_3)]dx_1dx_2dx_3, \tag{41}$$

where t is the number of sub-polyhedra in the one eighth of the polyhedral inclusion, and $(S_T)_{ijkl}$ is the Eshelby tensor at point $\mathbf{x}$ inside Ω_T given in Eqs. (9a), (37a), (37b), (37c) and (37d).

4. Numerical results

To illustrate the general formulas of the Eshelby tensor for a p-faced polyhedral inclusion of arbitrary shape derived in Section 3, three types of polyhedral inclusions (i.e., cubic, octahedral and tetrakaidecahedral) shown in Fig. 5 are quantitatively studied in this section. Cuboids are the first polyhedral inclusions investigated using classical elasticity (e.g., Chiu, 1977; Lee and Johnson, 1978; Liu and Wang, 2005). A tetrakaidecahedron can be generated by uniformly truncating the six corners of an octahedron and is known to be the only polyhedron that can pack with identical units to fill space and nearly minimize the surface energy (e.g., Li et al., 2003). Tetrakaidecahedral cells have been frequently used to represent foamed materials and interpenetrating phase composites (e.g., Li et al., 2003, 2006; Jhaver and Tippur, 2009).

Two components, S_{1111} and S_{1212}, of the Eshelby tensor at any point $\mathbf{x}$ inside each polyhedral inclusion with various sizes are evaluated using Eqs. (9a), (37a), (37b), (37c), (37d), (28) and (31) and plotted to demonstrate how the components change with the position and inclusion size. Also, how the average Eshelby tensor component $\overline{S}_{1111}$ varies with the inclusion size is presented here, which is computed using Eq. (41). For illustration purposes, Poisson's ratio v is taken to be 0.3 and the material length scale parameter L to be 17.6 μm in the current numerical analysis, as was done earlier (Gao and Ma, 2009, 2010a,b; Ma and Gao, 2010, 2011).

The distributions of S_{1111} for the cubic, octahedral, and tetrakaidecahedral inclusions along the x_1 axis predicted by the current model are shown in Figs. 6–8, where the values of S_{1111}^C are also displayed for comparison.

It can be seen from Figs. 6–8 that the classical part S_{1111}^C (based on classical elasticity) varies with the position of $\mathbf{x}$ within each polyhedral inclusion rather than uniform, which shows that the Eshelby conjecture is true for the three polyhedral inclusion shapes considered here. Also, it is found that for each of the three inclusion shapes S_{1111}^C at a given value of x_1/R is the same for all values of R/L, confirming the inclusion size-independence of the classical part of the Eshelby tensor, which is noted near the end of Section 3.1. In addition, for all three polyhedral inclusion shapes considered, it is observed from Figs. 6–8 that when the characteristic inclusion size R (see Fig. 5) is small (compared to the length scale

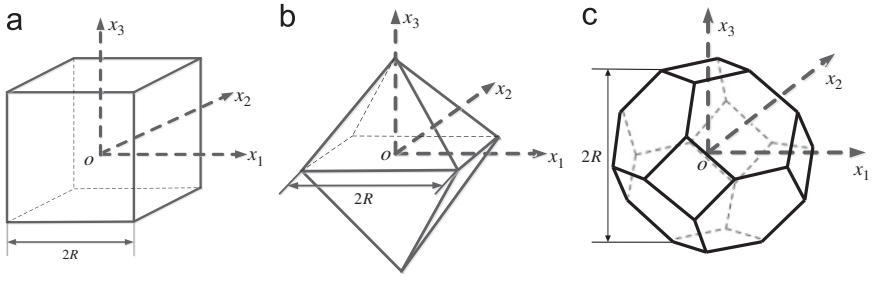

Fig. 5. Three types of polyhedral inclusions: (a) cubic, (b) octahedral and (c) tetrakaidecahedral.

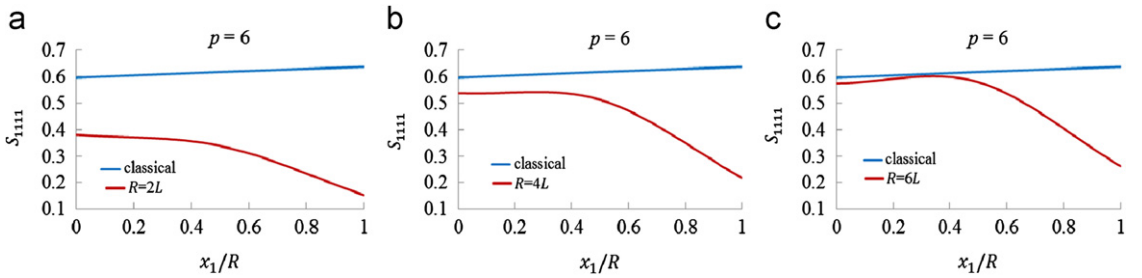

Fig. 6. Variation of S_{1111} along the x_1 axis inside the cubic inclusion: (a) $R=2L$, (b) $R=4L$ and (c) $R=6L$, with R being half of the edge length (see Fig. 5(a)).

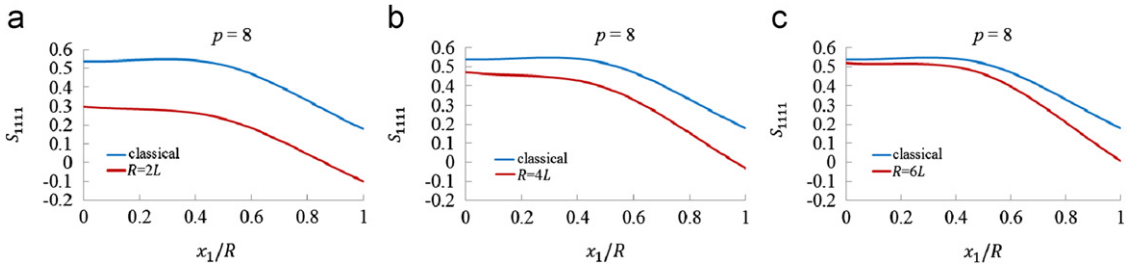

Fig. 7. Variation of S_{1111} along the x_1 axis inside the octahedral inclusion: (a) $R=2L$, (b) $R=4L$ and (c) $R=6L$, with R being half of the edge length (see Fig. 5(b)).

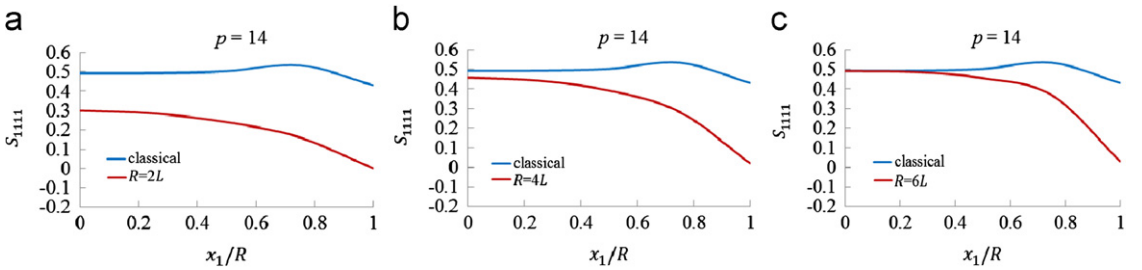

Fig. 8. Variation of S_{1111} along the x_1 axis inside the tetrakaidecahedral inclusion: (a) $R=2L$, (b) $R=4L$ and (c) $R=6L$, with R being half of the cell height (see Fig. 5(c)).

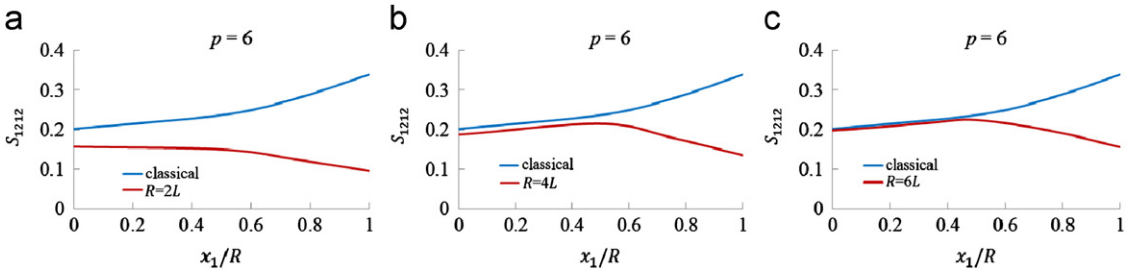

Fig. 9. Variation of S_{1212} along the x_1 axis inside the cubic inclusion: (a) $R=2L$, (b) $R=4L$ and (c) $R=6L$, with R being half of the edge length (see Fig. 5(a)).

parameter L, e.g., $R/L=2$), the strain gradient part S^G_{1111}, which is the difference between S_{1111} and S^C_{1111} (i.e., $S^G_{1111}=S_{1111}-S^C_{1111}$) and is displayed as the vertical distance between the S^C_{1111} curve and each S_{1111} curve in Figs. 6–8, is significant and should not be neglected. However, as the inclusion size becomes larger, the values of S_{1111} are all getting closer to those of S^C_{1111}. This means that the inclusion size effect is less significant and may be ignored for large inclusions in some cases, which agrees with the general trend observed experimentally (e.g., Cho et al., 2006).

The change of S_{1212} with the position and inclusion size is illustrated in Figs. 9–12 together with a comparison with S^C_{1212} for the three types of polyhedral inclusions. Clearly, S^C_{1212} varies with the position of $\mathbf{x}$ inside each polyhedral inclusion, which differs from that in an ellipsoidal inclusion and supports the Eshelby conjecture. But the classical part S^C_{1212} at a given value of x_1/R remains the same for all inclusion sizes, as expected from the discussion in Section 3.1.

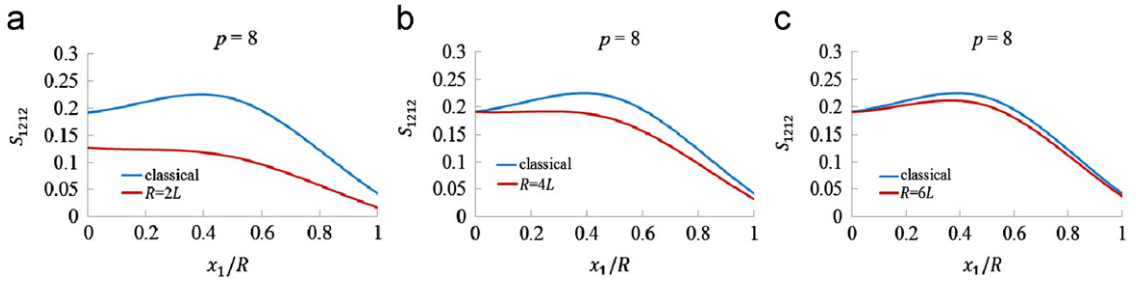

Fig. 10. Variation of S_{1212} along the x_1 axis inside the octahedral inclusion: (a) $R=2L$, (b) $R=4L$ and (c) $R=6L$, with R being half of the edge length (see Fig. 5(b)).

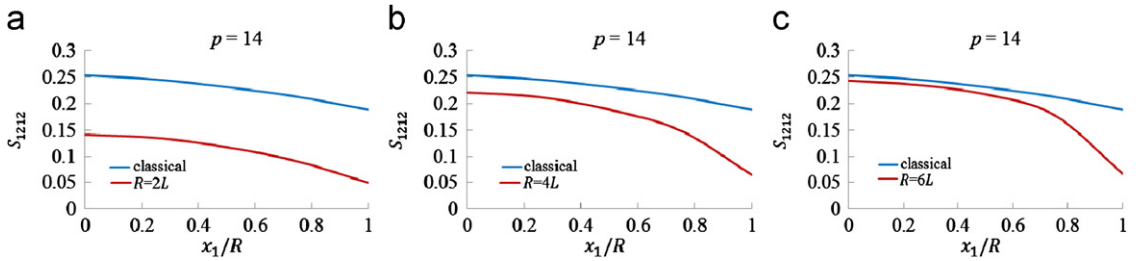

Fig. 11. Variation of S_{1212} along the x_1 axis inside the tetrakaidecahedral inclusion: (a) $R=2L$, (b) $R=4L$ and (c) $R=6L$, with R being half of the cell height (see Fig. 5(c)).

The gradient part S^G_{1212}, as the difference between S_{1212} and S^C_{1212} (i.e., $S^G_{1212}=S_{1212}-S^C_{1212}$), is seen to be significantly large for small inclusions (e.g., $R/L=2$) and becomes insignificant for large inclusions for all three types of polyhedral inclusions. More specifically, it is observed from Fig. 9 that for the cubic inclusion the strain gradient effect, as measured by the value of S^G_{1212}, is large for all inclusion sizes when $x_1/R>0.6$. For the octahedral inclusion, the strain gradient effect is insignificant and can be neglected when $R/L>4$, as illustrated in Fig. 10. For the tetrakaidecahedral inclusion, Fig. 11 shows that the strain gradient effect is also small, especially in the region away from the square faces.

The component $\overline{S}_{1111}$ of the averaged Eshelby tensor varying with the inclusion size is shown in Fig. 12 for the three inclusion shapes, where $\overline{S}^C_{1111}$ is also displayed for comparison. The values of $\overline{S}_{1111}$ shown in Fig. 12 are obtained using Eqs. (41) and (39a), (39b), (39c) and (39d), which are also applied to get the values of $\overline{S}^C_{1111}$ with $L\to 0$.

It can be seen from Fig. 12 that for each polyhedral inclusion $\overline{S}^C_{1111}$ (based on classical elasticity) is a constant independent of the inclusion size R. However, $\overline{S}_{1111}$ predicted by the current model based on the strain gradient elasticity theory does vary with the inclusion size: the smaller the inclusion, the smaller the Eshelby tensor component. In particular, when the inclusion is small, the strain gradient effect, as measured by $\overline{S}^G_{1111}(=\overline{S}_{1111}-\overline{S}^C_{1111})$, is significantly large and should not be ignored. As the inclusion becomes large, $\overline{S}_{1111}$ approaches $\overline{S}^C_{1111}$ from below, indicating that the strain gradient effect gets small and may be neglected for very large inclusions.

The observations made here are also true for the other components of the Eshelby tensor S_{ijkl} in Eqs. (9a), (37a), (37b), (37c), (37d), (28) and (31) and its volume average $\overline{S}_{ijkl}$ in Eq. (41).

From the numerical results presented above, it is clear that the newly obtained Eshelby tensor based on the SSGET can capture the inclusion size effect at the micron scale, while the Eshelby tensor based on classical elasticity does not have this capability.

5. Conclusions

An analytical solution is provided for the Eshelby-type problem of an arbitrarily shaped polyhedral inclusion embedded in an infinite elastic matrix using a simplified strain gradient elasticity theory (SSGET) that contains one material length scale parameter in addition to two classical elastic constants. The SSGET-based Eshelby tensor for a polyhedral inclusion of arbitrary shape is analytically derived in a general form in terms of three potential functions, two of which are the same as the ones involved in the Eshelby tensor based on classical elasticity. These potential functions, as three volume integrals over the inclusion, are evaluated by dividing the polyhedral inclusion domain into tetrahedral duplexes. Each of the three volume integrals is first transformed to a surface integral by applying the divergence theorem, which is then transformed to a contour (line) integral based on Stokes' theorem and using an inverse approach that differs from those employed in the existing studies based on classical elasticity. The newly obtained Eshelby tensor is separated into a classical part and a gradient part. The classical part depends only on Poisson's ratio of the matrix material, while the gradient part depends on

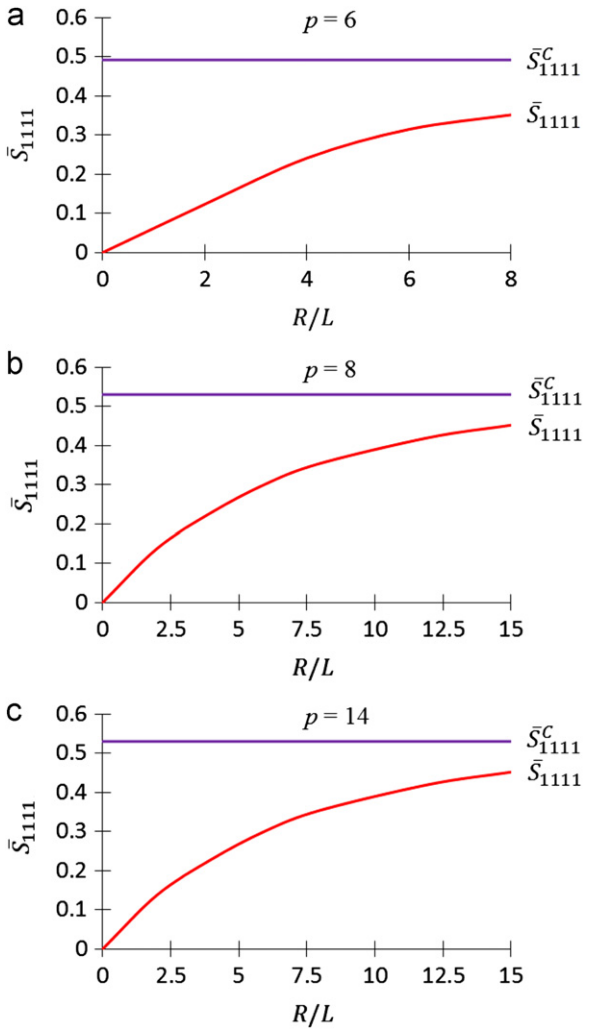

Fig. 12. Variation of $\bar{S}_{1111}$ with the inclusion size: (a) cubic, (b) octahedral and (c) tetrakaidecahedral.

both Poisson's ratio and the material length scale parameter that enables the explanation of the inclusion size effect. This SSGET-based Eshelby tensor reduces to its counterpart based on classical elasticity when the strain gradient effect is not considered. A general form of the volume averaged Eshelby tensor over the polyhedral inclusion is also obtained, which can be used in homogenization analyses of composites containing polyhedral inclusions.

To demonstrate the newly derived Eshelby tensor, three types of polyhedral inclusions, cubic, octahedral and tetrakaidecahedral, are analyzed by directly applying the general formulas. The numerical results reveal that for each of the three inclusion shapes the components of the new Eshelby tensor change with the position and inclusion size, whereas their classical elasticity-based counterparts only vary with the position. When the inclusion is small, the gradient part is seen to contribute significantly and should not be ignored. Also, it is found that the smaller the inclusion size is, the smaller the components of the volume-averaged Eshelby tensor are. These components approach from below the values of their classical elasticity-based counterparts as the inclusion size becomes large. Hence, the inclusion size effect may be neglected for large polyhedral inclusions in some cases.

Acknowledgments

The work reported here is funded by a Grant from the U.S. National Science Foundation (NSF), with Dr. Clark V. Cooper as the program manager, and by a MURI Grant from the U.S. Air Force Office of Scientific Research (AFOSR), with Dr. David Stargel as the program manager. The support from these two programs is gratefully acknowledged. The authors also would like to thank Professor Huajian Gao and two anonymous reviewers for their encouragement and comments on the paper.

References

Ammari, H., Capdeboscq, Y., Kang, H., Lee, H., Milton, G.W., Zribi, H., 2010. Progress on the strong Eshelby's conjecture and extremal structures for the elastic moment tensor. J. Math. Pures Appl. 94, 93–106.

Chiu, Y.P., 1977. On the stress field due to initial strains in a cuboid surrounded by an infinite elastic space. ASME J. Appl. Mech. 44, 587–590.

Cho, J., Joshi, M.S., Sun, C.T., 2006. Effect of inclusion size on mechanical properties of polymeric composites with micro and nano particles. Compos. Sci. Technol. 66, 1941–1952.

Eshelby, J.D., 1957. The determination of the elastic field of an ellipsoidal inclusion, and related problems. Proc. R. Soc. London A 241, 376–396.

Eshelby, J.D., 1959. The elastic field outside an ellipsoidal inclusion. Proc. R. Soc. London A 252, 561–569.

Eshelby, J.D., 1961. Elastic inclusions and inhomogeneities. In: Sneddon, I.N., Hill, R. (Eds.), Progress in Solid Mechanics, vol. 2. North-Holland, Amsterdam, pp. 89–140.

Gao, X.-L., Ma, H.M., 2009. Green's function and Eshelby's tensor based on a simplified strain gradient elasticity theory. Acta Mech. 207, 163–181.

Gao, X.-L., Ma, H.M., 2010a. Solution of Eshelby's inclusion problem with a bounded domain and Eshelby's tensor for a spherical inclusion in a finite spherical matrix based on a simplified strain gradient elasticity theory. J. Mech. Phys. Solids 58, 779–797.

Gao, X.-L., Ma, H.M., 2010b. Strain gradient solution for Eshelby's ellipsoidal inclusion problem. Proc. R. Soc. A 466, 2425–2446.

Gao, X.-L., Park, S.K., 2007. Variational formulation of a simplified strain gradient elasticity theory and its application to a pressurized thick-walled cylinder problem. Int. J. Solids Struct. 44, 7486–7499.

Gao, X.-L., Rowlands, R.E., 2000. Hybrid method for stress analysis of finite three-dimensional elastic components. Int. J. Solids Struct. 37, 2727–2751.

Glas, F., 2001. Elastic relaxation of truncated pyramidal quantum dots and quantum wires in a half space: an analytical calculation. J. Appl. Phys. 90, 3232–3241.

Jhaver, R., Tippur, H., 2009. Processing, compression response and finite element modeling of syntactic foam based interpenetrating phase composite (IPC). Mater. Sci. Eng. A 499, 507–517.

Kuvshinov, B.N., 2008. Elastic and piezoelectric fields due to polyhedral inclusions. Int. J. Solids Struct. 45, 1352–1384.

Lee, J.K., Johnson, W.C., 1978. Calculation of the elastic strain field of a cuboidal precipitate in an anisotropic matrix. Phys. Status Solidi (a) 46, 267–272.

Li, K., Gao, X.-L., Roy, A.K., 2003. Micromechanics model for three-dimensional open-cell foams using a tetrakaidecahedral unit cell and Castigliano's second theorem. Compos. Sci. Technol. 63, 1769–1781.

Li, K., Gao, X.-L., Subhash, G., 2006. Effects of cell shape and strut cross-sectional area variations on the elastic properties of three-dimensional open-cell foams. J. Mech. Phys. Solids 54, 783–806.

Li, S., Wang, G., 2008. Introduction to Micromechanics and Nanomechanics. World Scientific, Singapore.

Liu, L.P., 2008. Solutions to the Eshelby conjectures. Proc. R. Soc. A 464, 573–594.

Liu, S., Wang, Q., 2005. Elastic fields due to eigenstrains in a half-space. ASME J. Appl. Mech. 72, 871–878.

Lubarda, V.A., Markenscoff, X., 1998. On the absence of Eshelby property for non-ellipsoidal inclusions. Int. J. Solids Struct. 35, 3405–3411.

Ma, H.M., Gao, X.-L., 2010. Eshelby's tensors for plane strain and cylindrical inclusions based on a simplified strain gradient elasticity theory. Acta Mech. 211, 115–129.

Ma, H.M., Gao, X.-L., 2011. Strain gradient solution for a finite-domain Eshelby-type plane strain inclusion problem and Eshelby's tensor for a cylindrical inclusion in a finite elastic matrix. Int. J. Solids Struct. 48, 44–55.

Marcadon, V., Herve, E., Zaoui, A., 2007. Micromechanical modeling of packing and size effects in particulate composites. Int. J. Solids Struct. 44, 8213–8228.

Markenscoff, X., 1998a. On the shape of the Eshelby inclusions. J. Elasticity 49, 163–166.

Markenscoff, X., 1998b. Inclusions with constant eigenstress. J. Mech. Phys. Solids 46, 2297–2301.

Michelitsch, T.M., Gao, H., Levin, V.M., 2003. Dynamic Eshelby tensor and potentials for ellipsoidal inclusions. Proc. R. Soc. London A 459, 863–890.

Mura, T., 1987. Micromechanics of Defects in Solids, second ed. Martinus Nijhoff, Dordrecht.

Nemat-Nasser, S., Hori, M., 1999. Micromechanics: Overall Properties of Heterogeneous Materials, second ed. Elsevier Science, Amsterdam.

Nenashev, A.V., Dvurechenskil, A.V., 2010. Strain distribution in quantum dot of arbitrary polyhedral shape: analytical solution. J. Appl. Phys. 107, 064322-1–064322-8.

Nozaki, H., Taya, M., 2001. Elastic fields in a polyhedral inclusion with uniform eigenstrains and related problems. ASME J. Appl. Mech. 68, 441–452.

Pearson, G.S., Faux, D.A., 2000. Analytical solutions for strain in pyramidal quantum dots. J. Appl. Phys. 88, 730–736.

Poniznik, Z., Salit, V., Basista, M., Gross, D., 2008. Effective elastic properties of interpenetrating phase composites. Comput. Mater. Sci. 44, 813–820.

Rodin, G.J., 1996. Eshelby's inclusion problem for polygons and polyhedra. J. Mech. Phys. Solids 44, 1977–1995.

Rowlinson, J.S., 1989. The Yukawa potential. Physica A 156, 15–34.

Timoshenko, S.P., Goodier, J.N., 1970. Theory of Elasticity, third ed. McGraw-Hill, New York.

Vollenberg, P.H.T., Heikens, D., 1989. Particle size dependence of the Young's modulus of filled polymers: 1. Preliminary experiments. Polymer 30, 1656–1662.

Waldvogel, J., 1979. The Newtonian potential of homogeneous polyhedra. Z. Angew. Math. Phys. 30, 388–398.

Wang, J., Michelitsch, T.M., Gao, H., Levin, V.M., 2005. On the solution of the dynamic Eshelby problem for inclusions of various shapes. Int. J. Solids Struct. 42, 353–363.